Politecnico di Torino

Master Thesis in Biomedical Engineering

Endovascular repair of the aneurysm of the abdominal aorta by Chimney technique: a focus on the hemodynamics

Supervisors: Umberto Morbiducci

Michaelis Xenos

Candidate: Laura Fazzini

Co-Supervisors: Diego Gallo

Paola Tasso

Cento canzoni e cento
tamburi per ritardare
l' arrivo del Sole, così
aspettare che il giorno ci
prenda portandoci dentro a
mille rumori.

Acknowledgements

Thanks to Professor Umberto Morbiducci and Professor Diego Gallo for giving me the opportunity to develop my thesis abroad, learning new methods and habits and supervising my work.

I would like to express my sincere gratitude to Professor Michaelis Xenos for having introduced me to his group and for having approached me and discovered the world of research which was dark and inaccessible to me before living a marvellous experience at the University of Ioannina. A sincere thanks to Akis for mentoring me on daily work and for always being present.

A thanks to the Engineer Paola Tasso for supported and helped me during this process in every moment, your advice has been precious for the development of this work and will remain for me guidelines to follow in the future.

Contents

Abstract

Abdominal aortic aneurysm (AAA) is a pathological, localized and permanent dilatation of abdominal aorta that leads to vascular wall weakening due to the loss of mechanical properties caused by collagen and elastin degradation. If vessel's diameter dilatation is larger than 3 centimeters the patient is subjected to a surveillance protocol with periodic follow-ups and if needed he has to be treated to prevent aneurysm rupture and patient's death.

There are two surgical techniques for AAA treatment, in particular: (1) the open surgical repair (OSR), which involves the insertion of a stent graft by an incision of the patient in the abdominal area and (2) the endovascular repair (EVAR), which involves the insertion of the device through two incision in the groin area. The aim of both techniques is to exclude the aneurysm from the bloodstream in order to restore the physiological lumen.

Endovascular technique presents many advantages in fact: (1) it is minimally invasive; (2) does not require total anesthesia; (3) recovery times are short and (4) presents a low mortality and morbidity rate. However, some patients are not suitable for this technique due to their complex anatomical features and thrombus formation risk and device migration do not guarantee a long term stability of the device. From literature it is clear that these post-operative adverse events are in some relation with the local reshaping and hemodynamic due to device insertion. In particular, in this study we focused on patients treated with Chimney EVAR (CEVAR) technology, a particular kind of endovascular prosthesis that can be used in emergency case that involves the insertion of a main channel within secondary stent grafts are located to supply the renal and mesenteric arteries.

The aim of this work is to analyze two pre-operative and one-month post implantation patient-specific models treated with CEVAR and study their hemodynamic behavior using Computational Fluid Dynamic (CFD) method. CFD is an attractive tool for

hemodynamic research, it is powerfully and extensively used to reach the knowledge of hemodynamics inside a 3D domain with and high spatial and temporal resolution.

Starting from Computed Angiographic Tomografy (CTA) scan images the 3D models are segmented using the software Materialise Mimics. The computational grid and its quality are carried out in a solid meshing commercial software ICEM CFD. In CFD it is important to discretize a complex geometry into a large number of smaller but regular elements to solve the Navier-Stokes equations. The fluid dynamic simulations are carried out using the commercial software ANSYS Fluent® that solves fluid motion equations applying the finite volume method.

Pre- and post-operative scenarios are simulated. Simulations have been carried out imposing, at the inlet section, a time dependent velocity profile and, at the outflow sections, two different boundary conditions: (1) a time-dependent pressure profile and (2) a zero pressure condition. On each model near-wall time-averaged hemodynamic descriptors are analyzed such as: Time Averaged Wall Shear Stress (TAWSS); Oscillatory Shear index (OSI) and Relative Residence Time (RRT). Moreover, hemodynamic quantities related to significant instants of the cardiac cycle (e.g. systole, deceleration and diastole) such as pressure and Wall Shear Stress (WSS) are analyzed.

Moving from the pre-operative situation to the post-operative one, the trend of the hemodynamic descriptors is different; close to the aneurysm there is a positive increase of the TAWSS which encourages the presence of a direct flow towards the distal position and an undisturbed hemodynamics. For both of the boundary conditions analyzed the trend of TAWSS is the same; there are different trends close to the renal arteries where there are localized points with high TAWSS (TAWSS > 8 Pa) maybe due to geometry reconstruction. Oscillatory Shear Index reveals the presence of oscillatory flow that can lead to disturbed hemodynamics, in the post-operative case its values are lower than those observed before aneurysm treatment. The area that undergoes the greatest transformation is the aneurysmal area where high OSI areas are observed before the operation. The results referred to Relative Residence Time are in line with those observed in OSI, therefore RRT decreases especially in the aneurysmal

sac from pre-operative to post-operative. The instantaneous quantities analyzed reveal different situations if the instants referred to systole, deceleration and diastole are analyzed. The pressure, in the preoperative situation, results to assume decreasing values between systole and diastole of about 3 orders of magnitude, however, within the single model the pressure values are homogeneous. On the contrary, in the post-operative situation the pressure assumes decreasing values from the proximal to the distal area, thus restoring the physiological trend of the pressure. The analysis of pressure in post-operative situations is related to the risk of stent migration and the appearance of endoleaks. The WSS after the operation is higher than the pre-operative ones, this is a positive characteristic because low WSS values are found in areas that may be subject to thrombus formation. The two different pressure conditions in outlet have led to different results in terms of pressure, in fact, in the case of outlet pressure profile, the pressure does not reach values close to zero but remains elevated. The above considerations are valid for both patients analyzed.

It can be concluded that the CEVAR technique has reported positive results in the treatment of abdominal aortic aneurysm in the supra-iliac subrenal position. Future work may include including more patients into the cohort of patients studied in order to make the results statistically acceptable and for design optimization purposes. In addition, other parameters could be analyzed such as the recirculation volume and the displacement force to study the risk of migration and understand better the risk of thrombus formation to which post-operative models are subject.

1 Introduction

1.1 Cardiovascular system

The cardiovascular system is the group of organs that carry out the function of transporting fluids to the cells of the organism for their maintenance. The cardiovascular system in humans consists of the heart, which acts like a pump, blood vessels, divided in veins and arteries and the blood.

The heart consists of four chambers, two upper chambers called atria and two lower chambers called ventricles. The right part, constituted by atrium and right ventricle, is called the venous part while the left part, formed by atrium and left ventricle, is the arterial part. The atria are divided by the interatrial septum while the ventricles are separated by the interventricular septum. The atria and ipsilateral ventricles are separated by valves, the tricuspid valve on the right and the mitral valve on the left. The valves regulate the passage of blood from the atrium to the ipsilateral ventricle. The right atrium receives non-oxygenated blood from the upper vena cava, lower vena cava and coronary sinus. The right ventricle is connected to the right atrium with the tricuspid valve and the pulmonary circulation through the pulmonary artery. The left atrium receives oxygenated blood from the pulmonary circulation through four pulmonary veins and is connected to the left ventricle by the mitral valve. The left ventricle delivers blood through the aortic valve into the aorta artery, which then branches into arteries of smaller diameter and supplies blood to all body compartments (Tittel, Anatomia funzionale).

The large circulation and the small circulation can be distinguished: the large circulation begins in the left ventricle where oxygenated blood is sent, through the aorta, into the tissues. Initially the speed of the blood is 500 mm/s while after passing through the arterioles and reaching the capillaries it is equal to 0.5 mm/s (Tittel, Anatomia funzionale). In the capillaries, oxygen and several metabolites pass to the periphery, while metabolic waste (carbolic anhydride) is introduced into the blood from the tissues. After capillaries the blood moves from the arterial system to the venous system. Venous system transports the blood rich in waste to the right half of the heart

where the great circulation ends. From the right atrium, the carbon-rich venous blood passes to the right atrium, then to the right ventricle and finally the pulmonary arteries where the blood reaches the walls of the alveoli that are surrounded by capillaries. This is the small circulation. Through the walls of the capillaries, carbon dioxide is released and oxygen is taken into the blood from the alveolar atmospheric air. The blood, rich in oxygen, reaches, through the pulmonary veins, the left half of the heart where the pulmonary circulation (small circulation) ends and the general circulation starts again (Tittel, Anatomia funzionale).

.

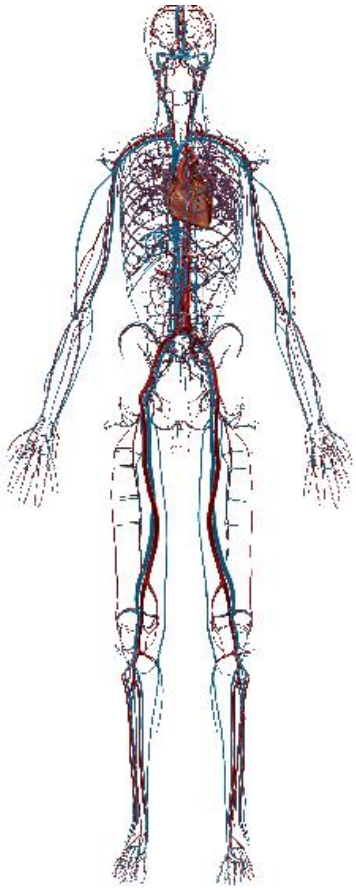

Figure 1. The cardiovascular system (Human Anatomy Atlas).

1.2 The heart

The heart is an involuntary muscular organ from which the blood circulation starts. It is hollow and has a conical shape.

The heart has approximately the size of a fist. In an adult man has a length of 14-16 cm, width of 12 cm and a thickness of 7 cm. In the non-trained subjects it has a weight of 350 g (Tittel, Anatomia funzionale).

It consists of three layers: endocardium, myocardium and epicardium. The endocardium is the inner part that comes int contact with the blood. The myocardium is the muscular part of the heart and has a pumping function. It has intermediate characteristics between smooth and striated muscles. The epicardium is an external coating.

The composition of the atria and ventricles is highly different due to the different pressure loads they have to support. The atria have an extremely thin musculature while the ventricles are organized into three layers of fibers that are then inserted on a fibrous skeleton.

During each cardiac cycle, the heart ejects 70 ml of blood at a pressure of 120 mm Hg into the aorta where the mean pressure is approximately 80 mmHg (Lasheras, 2007).

The heart receives non-oxygenated blood from the upper and lower vena cava that reach the right atrium, the blood, through the tricuspid valve, arrives in the right ventricle where it is pumped in the pulmonary circulation. The blood reaches the lungs where oxygenated and goes to the left atrium through the pulmonary vein. The mitral valve allows the blood flow in the left ventricle that is pumped in the aorta.

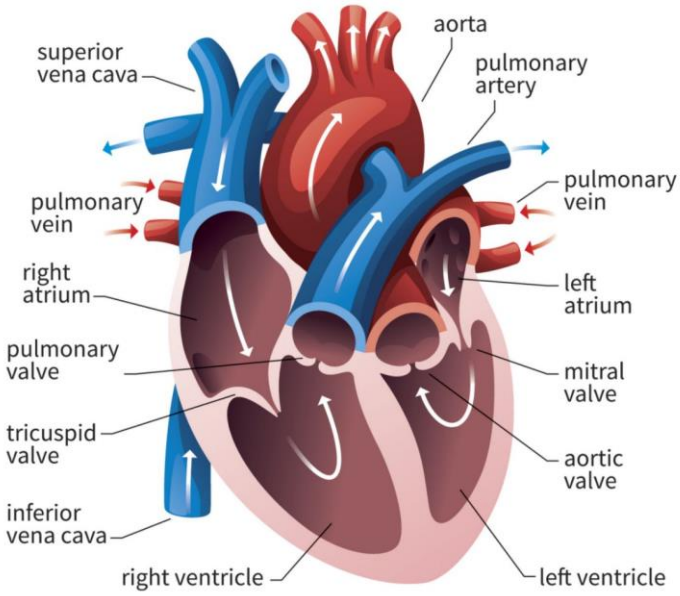

Figure 2. The heart (Bailey, Anatomy of the heart: valves).

1.3 Blood vessel

According to Azuma and Asegawa's theory, blood vessels are composed of:

- muscle: small step helical structure; provides stiffness and structure, has a high hysteresis loop under cyclical load conditions, the relaxation property tends to zero for long times.
- elastin: sheet with longitudinal openings; provides linear elastic stretch, has a low hysteresis, modulus of elasticity (1 MPa) and assures proportionality between stress and deformation; and low relaxation feature.
- collagen: disordered and rippled network in conditions of low stress, with the increase of stress new fibers are recruited, they are ordered and extended progressively. In conditions of high stress, it offers smoothness and strength, elastic modulus of the order of 1 GPa. Determines moderate hysteresis, so the behavior is not linear (Morbiducci, 2018).

Veins and arteries have a very different behavior due to their composition.

The arteries, as the distance from the heart increases, show up:

- decrease in diameter
- wall thickening
- decreasing of the elastic component and increasing of the muscle component in the tunica media.

The veins, as the distance from the heart increases, show up:

- decrease in diameter
- wall thinning.

Compared to arteries, veins have a lower content of elastin and smooth muscle cells as they have to tolerate lower blood pressure loads and do not return energy to propagate the stimulus.

The arteries are able to withstand loads of 1 order of magnitude greater than the veins. The reference for the arteries is 180 mmHg and for the veins 30 mmHg (Morbiducci, 2018)

The circulatory system is composed by veins and arteries. The arteries have been classified into large, medium, small arteries and capillary. They consist of:

- intima tunic: it is the inner layer and allows to separate the blood from the thrombogenic tissues.

- basal lamina: it has a structural function, it is made up of thrombogenic collagen, proteoglicans, elastin and glycoproteins, it serves as a filter and as a structure.

- medium tunic: it consists of smooth muscle cells and elastic fibers. It is the muscle layer of the vessel so it must propel the heart impulse. The smooth muscle cells regulate vasoconstriction and vasodilatation.

- adventitia tunic: made up of fibroblasts, elastic fibres, nerves and vasa vasorum which serve to spray the vessels themselves.

- external elastic lamina: similar to the basal lamina (Morbiducci, 2018).

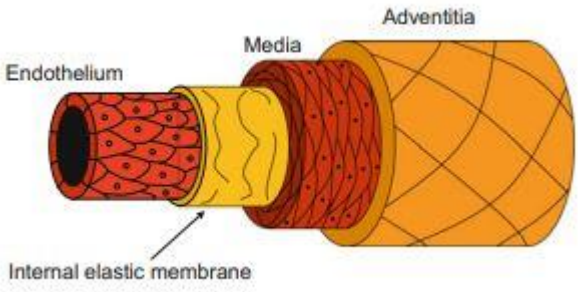

Figure 3. Blood vessel wall (Hoskins, 2017).

1.4 The blood

Blood is a tissue consisting of a suspension of elements in aqueous solution. The aqueous solution is called plasma (Morbiducci, 2018).

All the corpuscular elements of the blood are derived from the hemocytoblast and are formed in the process of hematopoiesis.

Erythrocytes, leukocytes and platelets are derived from hemocytoblast (Morbiducci, 2018).

Blood has the following functions:

- transport of oxygen through hemoglobin contained in erythrocytes and removal of carbon dioxide
- transport of nutrients and collection of waste from the various apparatus
- body temperature regulation: thermoregulation
- transport of hormones, enzymes and vitamins
- protection of the organism through white blood cells

- immediate repair of wounds through coagulation while awaiting the intervention of long-term mechanisms of regeneration.

1.4.1 Herythrocytes

Erythrocytes are small cells without a nucleus, with a diameter of about 8 μm and have the shape of a biconcave disk with a membrane around it called stroma. The membrane provides plasticity and transmembral performance, it is affected by all the fluid dynamic stresses of motion. The membrane is flexible, this capacity has a great impact on the flow capacity of the blood because it can withstand a minimum of resistance.

Inside the erythrocytes there is the cytoplasm, inside it there is a solution of hemoglobin, a protein able to bond oxygen in a reversible way. Each hemoglobin has four heme groups so four molecules of oxygen can be transported (Morbiducci, 2018).

The concentration of oxygen in the blood can be expressed as by the relation:

$$ct[02]=[O2]+[HbO2]$$

where

- [O2]→concentration of dissolved oxygen in plasma and globular liquid.
- [O2]= αO2pO2
- αO2→coefficient of solubility of oxygen in the blood
- [HbO2] Oxygen bonded oxyhemoglobin concentration.

1.4.2 Leoucocytes

Leukocytes are an aggregate of many elements, they have a spheroidal shape, a nucleus and, because of the presence of the nucleus, they are less deformable than red blood cells. They have antimicrobial function. There are several types of leukocytes:

- monocytes: in the case of inflammation, they migrate from the blood vessels and begin an activity of phagocytosis. They also have secretory function of defensive substances.

- granulocytes: they can be of different types; neutrophils that phagocyte microbes, basophils that release
- anticoagulants or vasodilators, have the function of creating hypersensitivity.
- lymphocytes: white blood cells that recognize and destroy antigens (Morbiducci, 2018).

1.4.3 Platelets

Platelets are spherical or oval-shaped corpuscles with a diameter of about 3µm. They are involved in clot deforming in immunological and inflammatory reactions of the internal walls of the vessels, they also block the passage of foreign agents into the blood stream (Morbiducci, 2018).

1.4.4 Plasma

Plasma is a slightly alkaline fluid made up of 90% water. The remaining 10% is made up of dissolved substances such as lipids, hormones, amino acids and carbohydrates. Inside the plasma there are also proteins, always in concentrations between 6.5 and 8 g/dl. Proteins carry the other dissolved substances. The main proteins are albumin, globulins and fibrinogen. Plasma proteins also determine the osmotic pressure of the blood.

1.5 Blood rheology

Rheology studies the sliding properties of materials (Morbiducci, 2018).

1.5.1 Blood density

The density of the blood considered as non-compressible fluid, is a function of the hematocrit and does not depend on the temperature and the state of motion. It can be calculated using the relation

$$\rho_s = (1 - Ht)\rho_p + Ht\rho_{gr}$$

where: ρ_s is the density of blood, $\rho_p$is the density of plasma, ρ_{gr} is the density of red cells, Ht is the hematocrit.

Usually, in physiological condition an adult with Ht = 45% has $\rho_s = 1060\ \frac{Kg}{m^3}$.

1.5.2 Blood viscosity

The viscosity of the blood, in the case of Newtonian fluid, depends on the temperature according to the relationship

$$\tau = \mu\dot{\gamma}$$

Where: τ is the yield stress, μ is the dynamic viscosity and $\dot{\gamma} = -\frac{\partial v_x}{\partial y}$ is the shear rate.

The unit of measurement of viscosity is cP where $1\text{cP} = 10^{-3}\text{Pa} * \text{s}$.

Blood includes substances with different phases in its composition so it cannot always be considered as a Newtonian fluid. The hypothesis of Newtonian fluid is valid only in large vessels up to the level of the arterioles, where the viscosity assumes values between 3 and 4 cP.

In addition to the size of the vessels, the viscosity of the blood is influenced by the shear rate. The shear rate is defined as the gradient of the velocity $\dot{\gamma}$.

The graph below shows the behavior of the blood and of a Newtonian fluid as the shear rate increases.

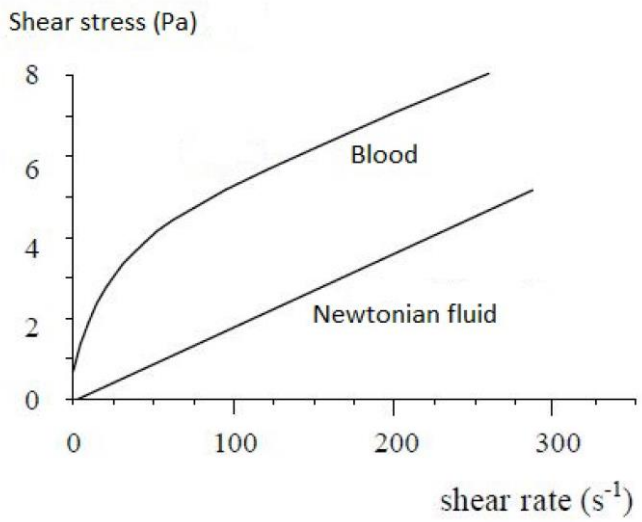

Figure 4. Behavior of blood and Newtonian fluid.

For $\dot{\gamma}$ range greater than 100 s^{-1} the blood behaves as Newtonian fluid.

In the case of large vessel and low shear rate the red blood cells congregate forming the rouleaux and affecting the viscosity.

In the case of small vessels and high shear rates the tangential stress avoids the accumulation of red blood cells (Morbiducci, 2018).

1.5.3 Non-Newtonian rheological model

Non-Newtonian fluids are fluids whose viscosity has a value that changes according to the shear stress applied, therefore the viscosity is not constant. A non-Newtonian fluid can be:

- Viscous

  → time dependent τ = f ($\dot{\gamma}$, τ_0, t) in this case it will never go back to the initial situation and the loading history will be maintained.

  → time independent τ = f ($\dot{\gamma}$, τ_0), after a certain period it will go back to the initial situation.

- Viscoelastic

  →it can strain but it maintains the previous load history.

The relationship for a non-Newtonian fluid is

$$\tau = \dot{\gamma}\mu_{app}$$

μ_{app} is not a physical property, it depends on the field of motion, $\mu_{app} \neq \mu$.

Some non-rheological models are:

1.5.4 Bingham model

The Bingham model follows the relation

$$\tau = \tau_0 + \dot{\gamma}\mu_B$$

Where: τ is the yield stress, τ_0 is the minimum yield stress to allow fluid motion, $\mu_B$is the Bingam dynamic viscosity and $\dot{\gamma} = -\frac{\partial v_x}{\partial y}$ is the shear rate

Bingham model is a good approximation of the behavior of the blood if $\dot{\gamma}$ is greater than 100 s^{-1} (Morbiducci, 2018).

Figure 5 below sums up the behavior of different fluids.

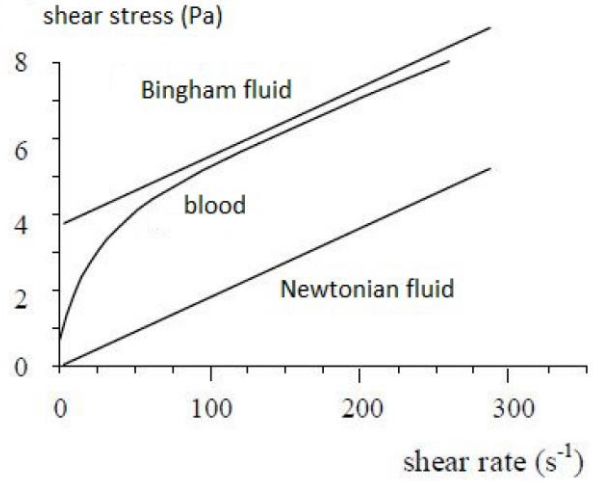

Figure 5. Bingham fluid behavior.

1.5.5 Casson model

Casson model is represented by the following relation

$$\sqrt{\tau} = \sqrt{\tau_0} + s\sqrt{\dot{\gamma}}$$

Where: τ is the yield stress, τ_0 is the minimum yield stress to allow fluid motion, $s = \sqrt{\mu_C}$ where μ_C is the Casson dynamic viscosity and $\dot{\gamma} = -\frac{\partial v_x}{\partial y}$ is the shear rate (Morbiducci, 2018).

1.5.6 Power Law model

The Power Law model follows the relation

$$\mu(\dot{\gamma}) = k(\dot{\gamma})^{n-1}$$

k flow consistency, it depends on hematocrit and plasma without albumin following an exponential relation

n power-law index, it linearly depends on hematocrit (Morbiducci, 2018).

1.5.7 Carreau model

The Carreau model follow the relation

$$\mu(\dot{\gamma}) = \mu_\infty + (\mu_0 - \mu_\infty)[1 + [(\lambda\dot{\gamma})^2]^{n-\frac{1}{2}}$$

where: λ is the relaxation time constant, μ_0 is zero shear stress limit viscosity, μ_∞ is the infinite shear stress limit viscosity, n is the power-law index, it linearly depends on hematocrit (Morbiducci, 2018).

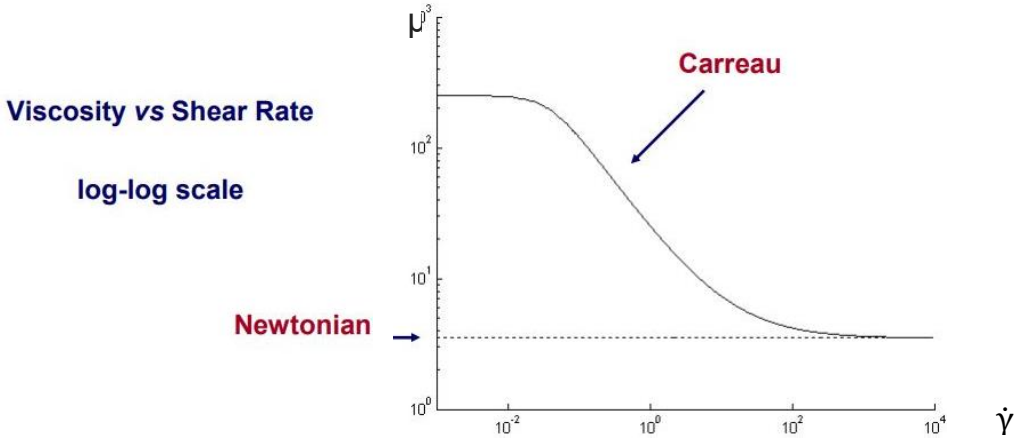

Figure 6. Casson fluid behavior.

1.6 Human aorta

The arterial system is composed by arteries, arterioles and capillaries in order of diameter size. The most important artery is the aorta. The aorta is the largest vessel in the body. The aortic root arises from the left ventricle of the heart, the aortic valve is the major portion of the aortic root that allows blood to flow from the heart to the whole body when it is open. The aortic valve also has the role of preventing back flow of blood into the heart when the valve is opened (Pornhatai et al, 2019).

Aorta originates from the left ventricle and after supplying the coronary arteries, has an initial tract called ascending aorta. It continues with the aortic arch where the arterial branches of the neck, head and upper limbs originate; it continues with a descending tract. The descending aorta is also called the thoracic aorta up to the level of the diaphragm, then it is called the abdominal aorta.

The abdominal aorta supplies the iliac arteries, renal arteries, arteries of the intestine, celiac trunk, upper and lower mesenteric arteries (Pornhatai et al, 2019).

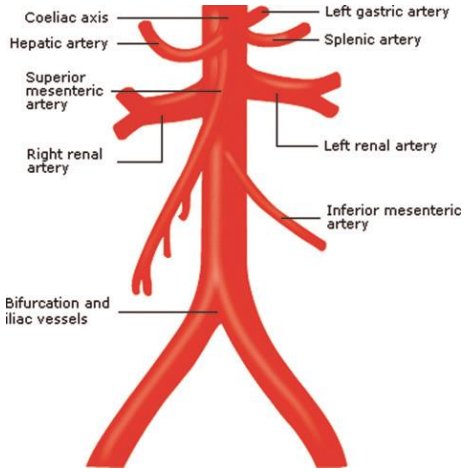

Figure 7. Abdominal aorta (Gedmintas A. et al., 2011).

During human life the body components are continuously regenerated to ensure the proper functioning of the body district. This process also takes place within the arteries. Sometimes, however, the wall of the arteries may weaken and no longer be regenerated; this phenomenon appears frequent in the abdominal and thoracic aorta. The causes can be traced back to multiple factors, in particular degeneration, biological and hemodynamic factors.

The aneurism is defined as the pathological, localized and permanent 50% dilation of an artery, with alteration of the wall and partial interruption of its elastic and muscular components (Lombardo et al, 2009/2010).

Following the formation of the aneurysm the resistance of the vessel walls decreases and therefore the vessel is no longer able to support the stress of the bloodstream. This can lead to the rupture of the aneurysm (Lasheras, 2007).

Two types of aneurysm can be distinguished: saccular and fusiform aneurism. Saccular aneurysms are common in the large cerebral arteries, while fusiform aneurysms are more prevalent in the abdominal aorta or in the arteries of the legs (Figure 8).

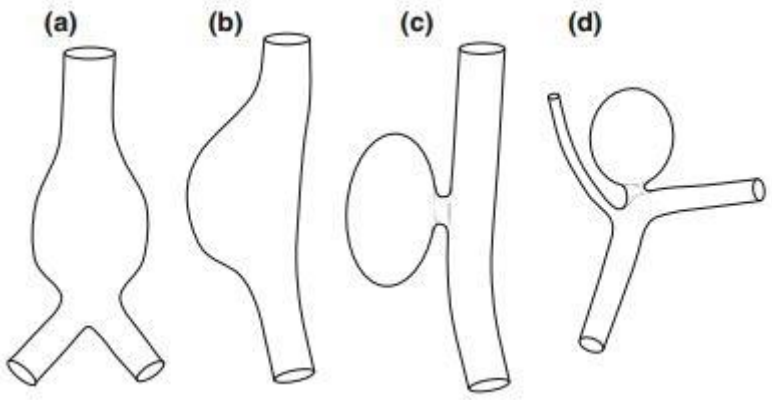

Figure 8. Fusiform and saccular aneurism: (a) and (b) fusiform aneurysm, (c) and (d) saccular aneurysm(Hoskins, 2017).

1.7 Open surgical repair and EVAR

An aneurysm can be treated in two different ways (Figure 9):

- OSR: open surgical repair technique
- EVAR: endovascular repair

OSR (Figure 9) is performed by making an incision in the abdomen, the blood flow in the aorta is momentarily blocked, the aneurism is opened and a fabric graft material is placed (Cooper A.,Endovascular repair of abdominal aortic aneurysm).

There are several potential risks and complication in OSR:

- Bleeding
- Infection of the graft
- Wound infection
- Heart attack
- Stroke
- Lung complications
- Death
- Spinal cord damages
- Sexual dysfunction after surgery

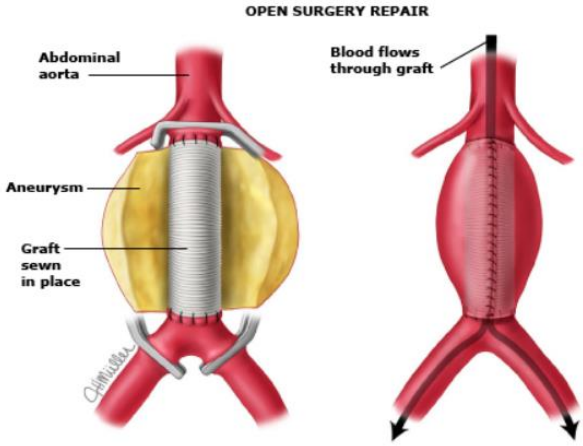

Figure 9. Open surgery repair of AAA (https://www.uptodate.com/contents/image?imageKey=PI%2F57520).

1.8 EVAR

EVAR is a mini invasive technique and it is performed by making two incision in the groin area and introducing the stent graft into the aorta. The stent graft is a synthetic tube, it also has a stainless-steel-scaffold attached to it in order to guide the stent inside the aorta. The stent is placed between two healthy portions of aorta and when it is in the proper position to allows the blood passing through it, bypassing the aneurysm. The stent increases the strength of the weakened walls and seals off the aneurysm.

The EVAR approach does not require surgery, so it is less invasive than OSR and provides a less dangerous option for patients who are deemed unfit for surgery. Unluckily long terms outcomes of EVAR are not still well known (Cooper, Endovascular repair of abdominal aortic aneurysm).

In the beginning, EVAR was offered only to patients at high operative risk. With evolution in device technology and technique, the application of EVAR has been broadened and is currently offered to patients with longer life expectancies (Dangas et al, 2012).

EVAR is available to patients with complex aortic anatomy through the development of customized stent grafts (Prinssen et al, 2003).

Potential risks and complications of endovascular repair include (Li et al, 2016):

- Bleeding
- Infection of the stent graft
- Surgical wound infection
- Leakage of blood from the graft into the aneurysm sac
- Graft movement or separation of components of the graft
- Kidney failure
- Death
- Nerve or spinal cord damage

The benefits of endovascular repair over traditional open surgery are:

- no large cuts in the abdomen
- no sutures (stitches), or sutures only at the groin area
- faster recovery and shorter time in the hospital
- less pain
- reduced complications (Prinssen et al, 2003).

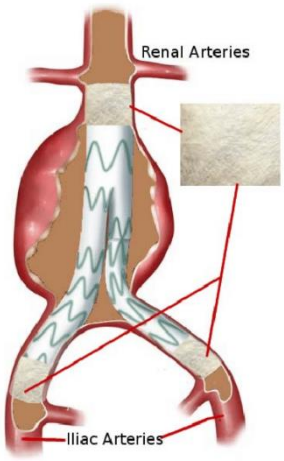

Figure 10. EVAR (Callan et al, 2011).

The decision between OSR and EVAR includes:

- aneurysm size and morphology
- patient age, general life expectancy and fitness for OSR

- the short- and long-term benefits and risks of the procedures including aneurysm-related mortality and operative mortality.

1.8.1 Complications due to endoprosthesis

Following surgeries involving endoprostheses, some complications may occur; the main complications are the migration of the prothesis that is a movement of the prothesis of at least 5 mm from the initial position, in that case a second operation is carried out, and the occlusion of the prothesis, it usually occurs 3 months after the surgery. Others problems related to the endoprothesis are the separation of the different portions of the endoprothesis that causes the filling of the aneurysmatic sac which then returns having a high risk of rupture, the rupture of the stent or of the hooks and the endoleak, it is the continuous flow in the sneurysmatic sac.

There are 5 different types of endoleak (Lombardo et al, 2009/2010):

- type 1:
  1a: failure to attach the prosthesis to the proximal neck
  1b: failure to attach the prosthesis to the distal neck
- type 2: reversal of blood flow in the arteries that supply the aneurysm (lumbar arteries and lower mesenteric artery), the aneurysmatic sac returns to fill up
- type 3: due to the separation of the grids that constitute the prosthesis
- type4: the prosthesis is porous or permeable.
- type 5: also called endotension, the pressure inside the aneurysm increases without any blood supply.

1.8.2 FEVAR

Fenestrated EVAR is a kind of stent graft usually custom made to suit the patient's anatomy. FEVAR are recommended in the case of patients with short proximal neck. This technique consists of implanting the main body of the stent which has fenestrations (holes) that allow the perfusion of the vessels that originate from the aorta. These vessels can also be strengthened through stents that join the main body at the fenestration (Li et al, 2016, Maldonado 2008).

1.8.3 CEVAR

The CEVAR technique was developed as a result of FEVAR to overcome the problem of the emergency; in fact, a patient who urgently needs endovascular treatment cannot use the FEVAR technique because it takes a period of time to manufacture the device. The manufacturing phase takes place after a careful preoperative analysis of the patient's geometry and all its parameters in order to have a custom-made device. The positions of the renal arteries and mesenteric arteries are particularly important because if the device is not correctly designed and manufactured there is a risk that the renal arteries or mesenteric artery will not be supplied with blood. On the other hand, CEVAR precedes the use of many endoprosthesis: the main body of the endoprosthesis is positioned inside the lumen and ends inside the iliac arteries; parallel to the main body, in an external position but always inside the vessel, secondary stents graft are positioned that run parallel to the main stent and then are inserted, at their respective heights, inside the renal arteries and mesenteric (Brant et al, 2015, Donas et al, 2012, Hiroshi et al, 2014, Kira et al, 2016, Pornhatai et al, 2019). In this way, the blood flow will also enter the secondary arteries that depart from the aorta. In the CEVAR technique it is the surgeon in the operating situation who positions the endoprosthesis according to the patient's geometry, which is however analysed in preoperative conditions. Before the surgery several parameters are analyzed in all types of EVAR, of particular importance are the aortic angle, the tortuosity and the presence of thrombus. Through these analyses and the criteria dictated by the guidelines, the degree of severity of the aneurysm is established. The presence of calcifications can affect the positioning of the endoprosthesis and prevent the passage of blood flow, these are classified by the guidelines as absent if less than 25% of the aortic segment. (Ohrlander et al, 2008, Sean et al, 2016, Walker et al, 2010). The tortuosity index is obtained by dividing L1 and L2 where L1 is the distance between the distal renal artery and the aortic bifurcation calculated on the ache line passing through the center of the lumen, L2 is the straight line between distal renal artery and aortic bifurcation (Walker et al, 2010). L aortic angle is evaluated as the most acute angle observed between distal renal artery and aortic bifurcation, on the center line.

The size of the proximal neck is also analyzed because it needs to provide a durable anchorage, the size and the tortuosity of the iliac arteries that need to provide access to the guide for stent placement and endoprosthesis. the iliac arteries are also studied because they need to remain pervie and provide a distal anchorage. CEVAR, in addition to being used in emergence situations, requires a shorter intervention time, less blood loss and exposure to fluorescent agents (Li et al, 2016, Morbiducci, 2018).

1.8.4 BEVAR

BEVAR are custom made stent grafts, they are stents with side branches that allow the inclusion of side vessels that depart from the aorta.

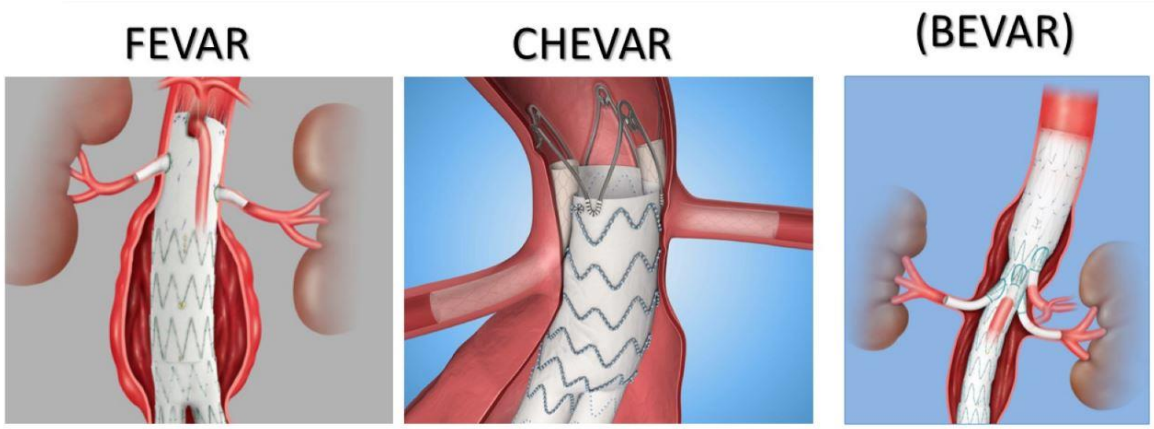

Figure 11. Different type of EVAR (Shawky, 2019).

1.9 State of the art

The aneurysm in the abdominal aorta is a swelling of the vessel wall that is mechanically weakened and structurally degraded. The abdominal aneurysm is continuously stimulated by the action of the blood that is ejected from the heart pump; in the event that the size of the aneurysm exceeds 1.5 times the physiological size of the vessel or 3 cm diameter (the physiological diameter of the aorta is 2 cm, if the diameter is about 5 cm the aneurysm is considered as large aneurysm), there may be rupture and internal bleeding, which may follow the death of the patient. In this case it is considered to be appropriate to treat the aneurysm (Desai et al, 2010).

Until 1991, the treatment for excellence of aneurysm was ORS (open repair surgery) characterized by a long period of convalescence for the patient, wounds in the abdomen and increased risk during the operation. In 1991, a new methodology for the treatment of aneurysm, EVAR, was introduced and is still being used and improved. Clinicians initially reported positive experiences with the use of stent graft. These devices consisted of a stent that was properly anchored, but which did not cure problems such as reflux and migration, so a subsequent ORS was required. In 1993 the first tube graft produced by Endovascular technologies (Guidant, Menlo Park, CA, USA) was implanted. After the development of this first device, another 15 stent grafts were produced and marketed, following several studies and clinical applications, some of which were withdrawn from the market because they were considered more dangerous than ORS.

The general structure of all stent grafts includes a tubular graft with an average diameter of 2-3 cm. This main structure is divided into two components with a smaller diameter that fit inside the iliac, in this case the device is called a bifurcated. If the device is a uni-iliac device, on the other hand, the main tubular stent reduces in diameter until it flows into a single iliac artery. These two types allow the device to be adapted to the patient's geometry. Today, although several stents have been produced, only six have obtained official approval from the FDA (Food and Drug Administration) to be used in EVAR: the AneuRx, Talent and Endurant (Medtronic Inc. Minneapolis, MN, USA), the Excluder (WL Gore and Associates, Flagstaff, AZ, USA), the Zenith (Cook Inc., Bloomington, IN, USA), and Powerlink (Endologix, Irvine, CA, USA).

EVAR stands for endovascular aneurysm repair; the technique involves the insertion of the stent graft through a mini-invasive procedure, less risky for the patient. Initially EVAR was used only in cases where it was not possible to treat with ORS due to patient’s complex anatomical features. Subsequently EVAR has been used more and more because of its excellent results in the medium and long term. The development of stent-graft for EVAR has seen the succession of four different periods: initially it was the physicians who did the graft, then the first industries of devices were developed, these have evolved to the intermediate phase and then to the modern one

(Xenos et al, 2019). Nowadays there are different types of EVAR: FEVAR, CEVAR and BEVAR.

The various alternatives associated with EVAR are designed to meet the needs of the patient looking towards a custom-made stent graft. A recent study (Xenos et al, 2007) showed that there were no substantial differences in the quality of life of patients treated with CEVAR or FEVAR, the choice depends on what the physician considers to be optimal for the patient and his needs; it should be noted that CEVAR can be done in emergency situations and requires basic tools while FEVAR needs high fabrication and intervention time (Decasse et al, 2016).

Nowadays from an engineering point of view, the behavior of blood flow inside the vessels can be studied in detail using CFD (computational fluid dynamic). The first steps for modern CFDs were taken in 1922, although Lewis Fry Richardson's project failed miserably. In 1957 several methods for simulating 2D flow were developed by the T3 group at Los Alamos National Lab. In 1967 John Hess and A.M.O. Smith published the first paper containing 3D models. In CFD modeling a complex geometry reconstructed from the real one is divided into many regular elements in which the solutions of the equations are then calculated. (Antiga et al, 2008).

In the last decade tools have been developed to study complex 3D blood patterns, which change with time. Following an accurate reconstruction of the geometry and the application of boundary conditions, the CFD allows to simulate and extract hemodynamic indices useful to prevent adverse events such as the migration of the stent, occlusion of the stent and the breakage due to excessive stress. This technique can help to make long-term evaluations on the device, showing undesirable aspects of blood flow that can lead to medical complications.

In a recent study the example of low WSS that can lead to the signing of a thrombus or the occlusion of arteries originating from the main one is reported (Xenos M. et al., 2019).

The computational approach is advantageous for its non-invasiveness, low cost, high analytical resolution and model customization. The computational approach can therefore be used both in the stent design phase and in the follow-up phase to analyze the post-operative situation. Nowadays there are still some limitations, the most important of which is the reconstruction of the geometry of the lumen that determines the hemodynamics and on which the computational simulation is based (Xenos et al, 2019).

2 Materials and methods

This chapter explains the methods used, starting from the acquisition of clinical images to the display of the results through the post processing operation. The steps taken and the software used for the various steps are explained in detail.

2.1 Study case

The study aims to analyse two pre- and post-operative patient-specific models treated with CEVAR endo-prosthesis. Both pre- and post-operative situations are analyzed in order to understand if the surgical technique improve, form an hemodynamic perspective, the pre-operative situation. The data are provided by the Department of Vascular Surgery of Larissa Hospital (Larissa, Greece). The patients gave their consent to the processing of personal data and privacy has not been violated. The images provided come from a Computed tomography angiography (CTA) analysis, the diagnosis by images is made thank to the injection of a contrast medium in order to distinguish the vessels tree. For the endovascular surgery an Endurant® stent graft (Medtronic Vascular, Santa Rosa, CA) was adopted. This device is modular and consists of multifilament polyester fabric and electropolished Nitinl utiliol stent (Malatos et al, 2019). The suprarenal anchor system includes a one-piece Nitinol stent with anchor pin while its first sealing stent is M shaped, providing neck conformability. All software necessary for reconstruction, simulation and visualization has been made available by the Mathematics Department of Ioannina University (Ioannina, Greece).

2.2 3D model reconstruction

Starting from CTA DICOM images, the 3D models are segmented and reconstructed using MIMICS® software package (Materialise, Leuven, Belgium). Initially the images are imported and the volume of interest (VOI) is selected that considers the area between the proximal suprarenal aorta and the common iliac up to the internal and external iliac bifurcation. Also, the reconstruction did not include small arteries, such as coeliac trunk and lower mesenteric artery in order to simplify the reconstruction. The segmentation does not consider aortic wall thickness. The presence of stent graft is reflected by the presence of radiopaque markers. Medical images are made up of

pixels that assume colors in the gray scale that reflects the different structures of the human body. In Figure 12 it is possible to visualize how a DICOM image appears immediately after the importation. To reconstruct the 3D model the images are segmented, the ROI is reconstructed using a mask applied slice by slice in order to analyse only the desired geometry. In the preoperative case, only one mask is used because there is only one structure to reconstruct. In MIMICS In the post-operative models multiple masks were used (4 masks in total):

- One for the reconstruction of the lumens of the aorta and iliac;
- One for the right renal artery;
- One for the left renal artery;
- One for the upper mesenteric artery

Figure 12 illustrates the process of reconstructing 3D models from the CT images provided by the clinicians

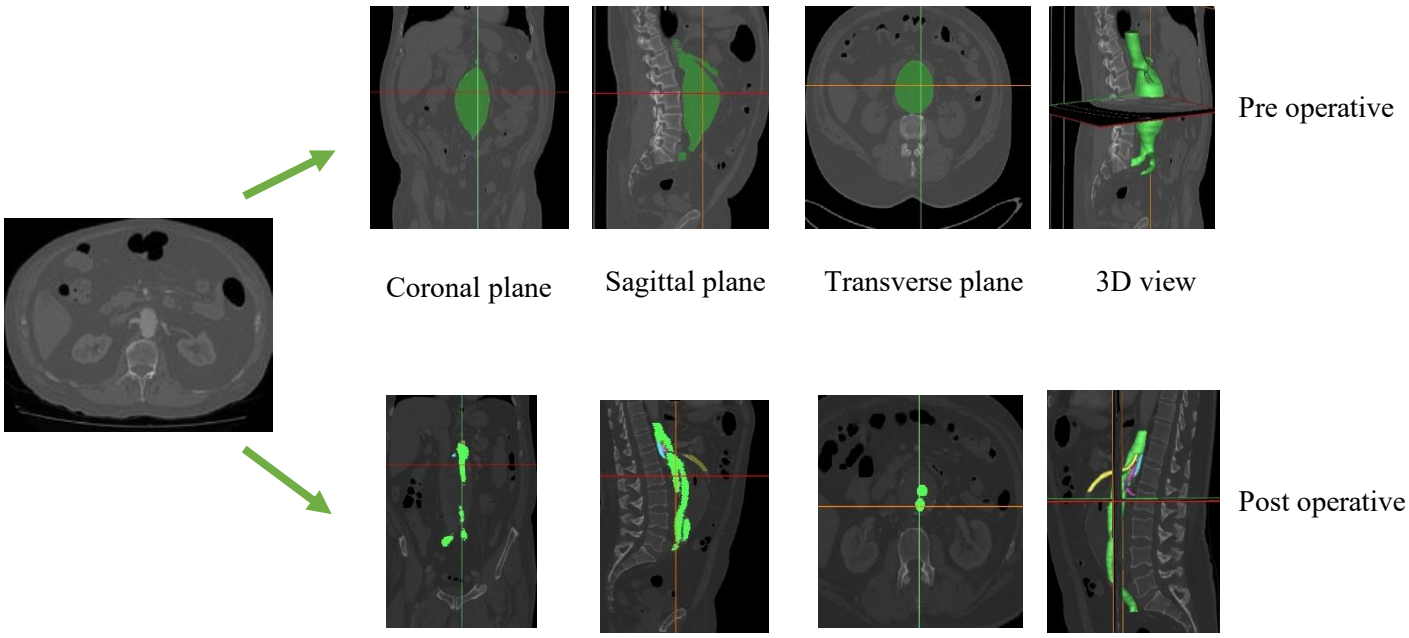

Figure 12. Image process reconstruction.

Following reconstruction, the models are affected by noise from CT scan artefacts. To improve the quality of the model and decrease errors, the models were filtered through a low-pass filter that performed the smoothing action. The smoothing values analysed

are those reported in Figure 13, Figure 14, Figure 15 where the percentage differences are reported for the different branches.

For each of these, the maximum, minimum and average distance from the centreline of the segments of the model (main lumen, right and left renal, right and left iliac) were studied and then the percentage differences were compared with the unsmoothed case.

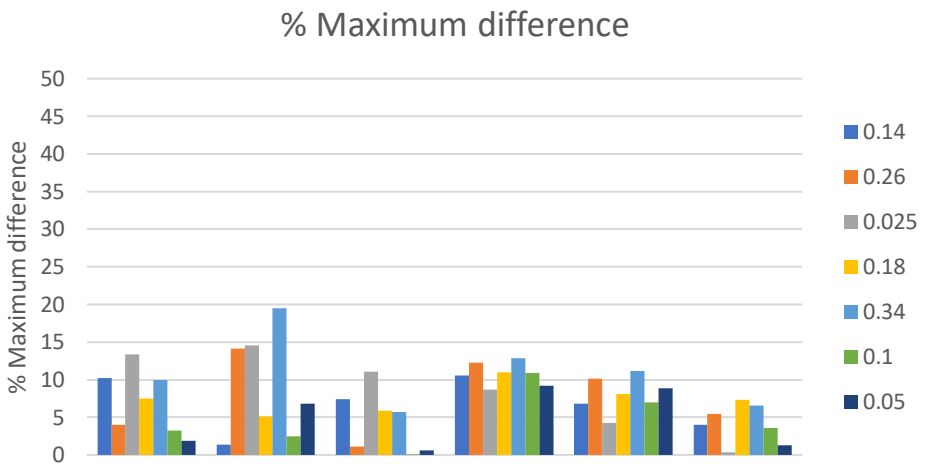

Figure 13. Maximum percentage difference between branches in smoothed and unsmoothed models.

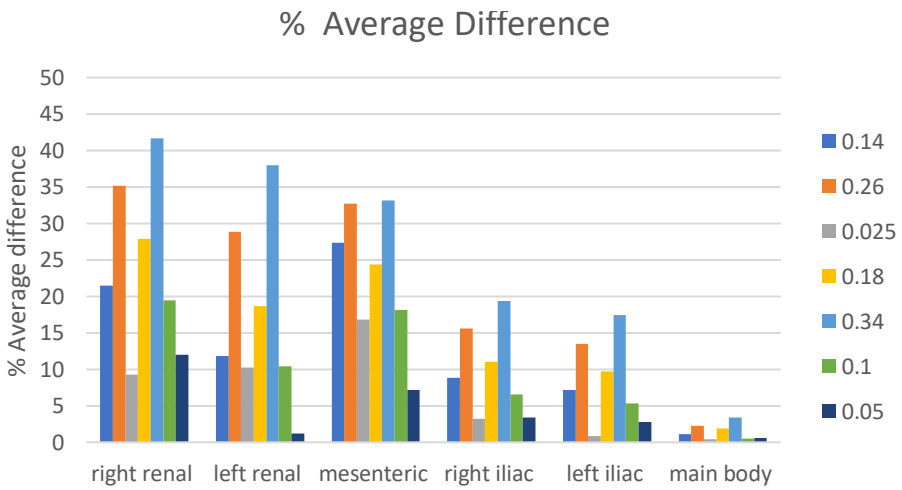

Figure 14. Average percentage difference between branches in smoothed and unsmoothed models.

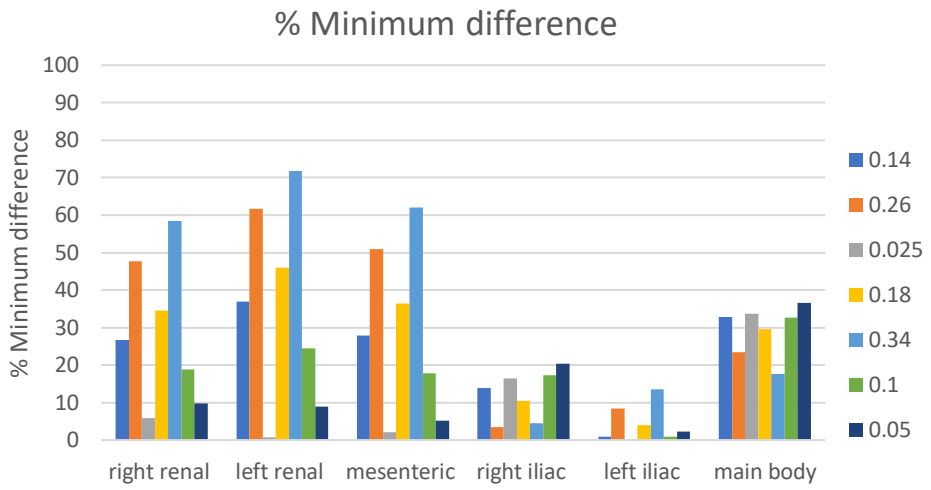

Figure 15. Minimum percentage difference between branches in smoothed and unsmoothed models.

The smoothing factor 0.050 is the one that provides the best compromise both from a visual analysis and by analysing the percentage differences. This smoothing value is used in both pre-operative and post-operative one month cases in order to provide comparable results.

At the end of the process, the 3D model saved in stereolitography (STL) file-format was created in MIMICS and imported into the Vascular Modelling Toolkit software (VMTK®). The geometry is further modified to prepare for fluid dynamics simulations: models are clipped in inlet and outlet regions so they are open and a flow extention is placed at the inlet section to ensure that the flow is fully developed once it reaches the region of interest.

Having a fully developed flow means that there are no adverse effects associated to the boundary conditions imposed in the inlet. The flow extention is set to 8 times the average of the inlet and outlet radius. In Figure 16 the final geometry is represented.

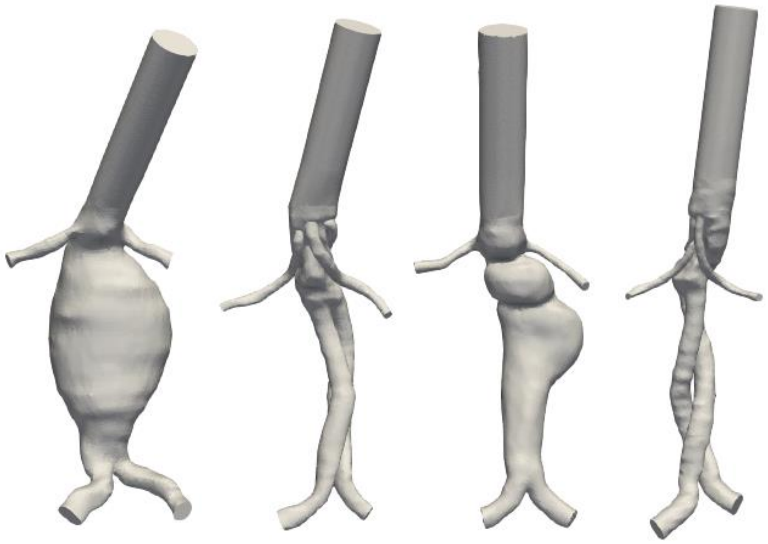

Figure 16. Rapresentation of the models after the addition of the flow extention.

Taking into consideration only the preoperative model where there are no stent grafts, the obtained model in .stl format was imported into ICEM CFD (Ansys Inc.,Canonsburg, PA). The initial physical domain has to be discretized in order to obtain sub-domains with smaller dimensions than the initial one to determine the solutions of the equations in an easier way.

In this study a 2 million element mesh has been considered. The size of the mesh elements could be further increased but, if on the one hand the accuracy of the solution increases a lot as the mesh size decreases, on the other hand the computational time increases exponentially together with the computational memory.

For post-operative cases, instead, an additional step was necessary, in particular lumen, right renal artery, left renal artery and upper mesenteric artery have to be correctly combined. After having performed all the operations performed in the preoperative case but before defining the mesh properties, the different surfaces are combined. Curves are created that outline the area of intersection between lumen and right renal artery, left renal artery and upper mesenteric artery. The surface of the lumen has been cut in correspondence of the curves previously created so as to create openings in the lumen to allow the insertion of the lateral arteries. Subsequently the four parts were merged in order to obtain a single surface. In Figure 17 the cut step is shown.

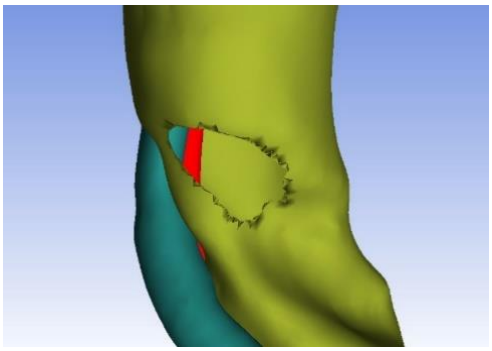

Figure 17. Model cut rapresentation.

After definition and computation of the mesh, it is smoothed and checked for incorrect elements.

Both in the pre operative and in the 1 month post operative case the mesh is subsequently improved until the quality of the mesh is at least 0.2, then it is imported into the commercial CFD code Fluent® (ANSYS Inc., Canonsburg, PA) where the simulations were performed on tetrahedral meshes.

2.3 Computational simulations

All fluid-dynamic simulations were performed using the finite volume method. The blood is considered as an homogeneous and incompressible Newtonian fluid with a density (ρ) equal to 1050 $^{kg}/_{m^3}$ and a dynamic viscosity equal to 0.0035 Pa·s. The wall was assumed rigid and a no-slip condition was imposed.

2.4 Navier-Stokes equations

The total volume of the models that are considered in this study can be divided into many fluid volumes on which the external forces acting on this volume can be of two different types: mass forces that are applied to the particles contained in the fluid volume and surface forces that are applied to the fluid particles that make up the surface (Lanzoni, Le equazioni della meccanica dei fluidi, Stergiopulos et al, 1992).

2.4.1 Conservation of the mass

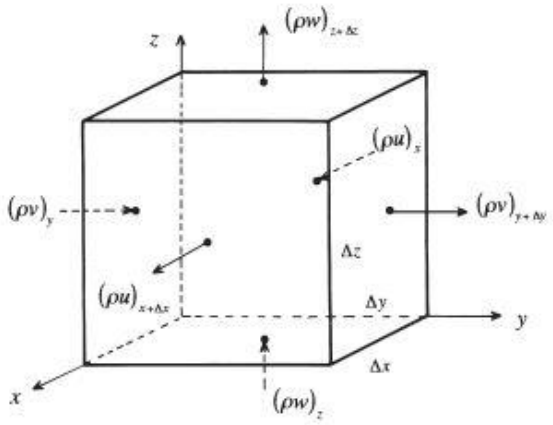

Figure 18. Fluid volume and mass force components.

The law of mass conservation states that in a closed volume in space the rate of increase of mass within the volume is equal to the net rate at which fluid enters across the surface of the volume (Pedley, 1997).

We consider a fluid volume as it is represented in Figure 2.5, the equations of conservation of the mass referred to the axes are written and the following equation is obtained:

$$(\Delta x \Delta y \Delta z)\frac{\partial \rho}{\partial t} = \Delta y \Delta z([\rho u]_x - [\rho u]_{x+\Delta x}) + \Delta x \Delta z\left([\rho v]_y - [\rho v]_{y+\Delta y}\right) + \Delta x \Delta y([\rho w]_z - [\rho w]_{z+\Delta z})$$

Dividing all the elements by $\Delta x \Delta y \Delta z$ the following equation can be obtained

$$\frac{\partial \rho}{\partial t} = -[\frac{\partial}{\partial x}(\rho u) + \frac{\partial}{\partial y}(\rho v) + \frac{\partial}{\partial z}(\rho w)$$

It can be even written as

$$\frac{D\rho}{Dt} = -\rho \nabla u$$

where

ρ is the density of a single fluid element and the value for the blood is 1050 $^{Kg}/_{m^3}$.

$\frac{D\rho}{Dt}$ is the rate of change of density of a single fluid element, u is the velocity, ∇u is divergence of the velocity field.

In this study the fluid is considered as incompressible so the density doesn't change so

$$\frac{D\rho}{Dt} = 0$$

from which follows the continuity equation

$$\nabla \cdot u = 0$$

2.4.2 Conservation of the momentum

The law of the momentum conservation states that the rate of momentum accumulation is equal to the sum of the rate of the incoming cementum, the rate of the outcoming momentum and the forces that act on the surface of the fluid volume that is considered. (Pedley, 1997).

The sum of the mass and surface forces acting on the fluid volume is defined as the product of the mass of the fluid element and its acceleration. (Pedley, 1997).

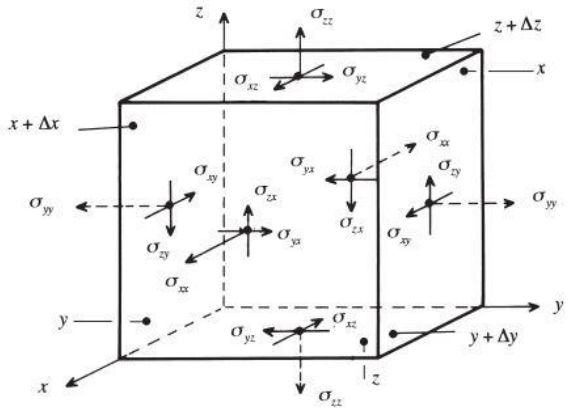

Figure 19. Fluid volume and surface force components.

Let's consider a fluid volume, the the force component acting on the faces of the volume in the direction perpendicular to the x-axis is written as

$$(\sigma_{xx}|_{x+\Delta x} - \sigma_{xx}|_x)\Delta y\Delta z$$

If the volume is small the following simplification can be done

$$(\sigma_{xx}|_{x+\Delta x} - \sigma_{xx}|_x)\Delta y\Delta z = \frac{\partial \sigma_{xx}}{\partial x}\Delta x\Delta y\Delta z$$

Similarly, the x components of the forces acting perpendicularly to the y-axis can be written

$$(\sigma_{xy}|_{y+\Delta y} - \sigma_{xy}|_y)\Delta x\Delta z = \frac{\partial \sigma_{xy}}{\partial y}\Delta x\Delta y\Delta z$$

As well as the x-component of the forces acting perpendicularly to the z-axis

$$(\sigma_{xz}|_{z+\Delta z} - \sigma_{xz}|_z)\Delta x\Delta y = \frac{\partial \sigma_{xz}}{\partial z}\Delta x\Delta y\Delta z$$

So component x of the Navier-Stokes equation can be written as

$$(\rho\Delta x\Delta y\Delta z)\frac{Du}{Dt} = (\rho g_x)\Delta x\Delta y\Delta z + (\frac{\partial \sigma_{xx}}{\partial x} + \frac{\partial \sigma_{xy}}{\partial y} + \frac{\partial \sigma_{xz}}{\partial z})\Delta x\Delta y\Delta z$$

By repeating the same procedure for all the components and dividing by the volume $\Delta x\Delta y\Delta z$ the generalized equations for the different components are obtained

$$\rho\frac{Du}{Dt} = \rho g_x + \nabla \cdot \sigma$$

The equation can be written by substituting the speed for stress σ obtaining the three Navier-Stokes equations

$$\rho \frac{Du}{Dt} = \rho g_x - \frac{\partial \mathrm{p}}{\partial \mathrm{x}} + \mu\left(\frac{\partial^2 u}{\partial x^2} + \frac{\partial^2 u}{\partial y^2} + \frac{\partial^2 u}{\partial x^2}\right)$$

$$\rho \frac{Dv}{Dt} = \rho g_y - \frac{\partial \mathrm{p}}{\partial \mathrm{y}} + \mu\left(\frac{\partial^2 v}{\partial x^2} + \frac{\partial^2 v}{\partial y^2} + \frac{\partial^2 v}{\partial x^2}\right)$$

$$\rho \frac{Dw}{Dt} = \rho g_z - \frac{\partial \mathrm{p}}{\partial \mathrm{z}} + \mu\left(\frac{\partial^2 w}{\partial x^2} + \frac{\partial^2 w}{\partial y^2} + \frac{\partial^2 w}{\partial x^2}\right)$$

The previous equations can be summarized as

$$\rho \frac{Du}{Dt} = \rho g - \nabla \mathrm{p} + \mu \nabla^2 u$$

where u is a vector and has its 3 components, $\rho \frac{Du}{Dt}$ is the inertial component of the equation, ρg represents the body force, $\nabla \mathrm{p}$ is the pressure gradient and $\mu \nabla^2 u$ represents the viscous component.

In this work the blood respects these laws and it is consideres as a fluid with Newtonian behavior, incompressible and homogeneous (Tittel, Anatomia funzionale dell'uomo, Lantz et al, 2013) that follows the equation of the conservation of the mass and the equation of Navier-Stokes.

$$\begin{cases} \nabla \cdot u = 0 \\ \rho \frac{Du}{Dt} = \rho g - \nabla \mathrm{p} + \mu \nabla^2 u \end{cases}$$

2.5 Poiseuille flow

The Poiseuille flow is a one-dimensional flow that respects the following assumptions (Morbiducci, 2019):

- Newtonian fluid: homogeneous and incompressible fluid, viscosity μ and density ρ constant
- Laminar flow

- No slip condition at the vascular wall
- Steady flow
- Cylindrical shape of the vessel
- Rigid wall
- Fully developed flow

These conditions are not fully met in reality due to the geometry that does not ensure a circular section and therefore a cylindrical shape of the vessel, a viscoelastic structure of the vessel wall, the flow is also pulsatile and not steady. Even if the assumptions are not completely respected, it is assumed that the blood behaves like a Poiseuille fluid. The fully developed profile is guaranteed at a certain distance from the inlet section when the equilibrium of the acting forces is obtained; a boundary layer δ is defined as the distance between the wall and the maximum velocity; when δ=R where R is the radius of the conduit has the fully developed motion. This condition is reached at an inlet length EL

$$\mathrm{EL} = 0.0065\mathrm{DRe}$$

where

D is the diameter of the vessel

Re is the Reynold's number

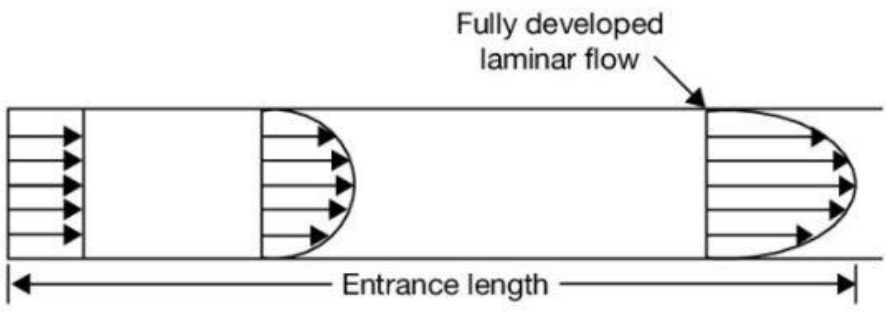

Figure 20. Entrance lenght rapresentation in the vessel.

the Reynold's number is the ratio between inertial forces and viscous forces, it is defined as

$$Re = \frac{\rho u D}{\mu} = \frac{inertial\ forces}{viscous\ forces}$$

Where: ρ is the density of the blood, u is the mean velocity in the cross section area, D is the diameter of the vessel and μ is the dynamic viscosity of the blood

The Reynolds number can assume different values and ranges are indicated to discriminate different types of flow; if se $Re < 2000$ the flow is laminar, if se $2000 < Re < 10000$ the flow is transitional and if se $Re > 10000$ the flow is turbulent. In this work the flow is considered laminar when the time and space available do not allow the transition to turbulent flow.

2.6 Wall properties

In order to obtain optimal results, the non-linearity and anisotropy of the vessel components should be considered. However, due to the high computational costs that this operation would require, the vessel wall is considered as rigid and the no slip condition is also imposed. The properties and thickness of the stent graft have not been taken into account (Xiao et al, 2012).

2.7 Numerical solution

Numerical simulations were performed in Ansys Fluent software packages (Ansys Inc., Canonsburg, PA) with the finite volume method. Simulations are performed for three cardiac cycles in two Intel Xeon processor (E5645, 2.40GHz, 12MB Cache, 5.86GT/s Intel QPI) of a Dell™ T7500 workstation. The only results that are connected to the last cardiac cycle were considered to avoid dynamic disturbances of numerical solution in the previous cycles, in this way the transitorio is not considered. The cardiac cycle was supposed to last $t = 1s$ with a fixed timestep of 0.001 s. The maximum number

of timesteps per cardiac cycle is set to 1000. Convergence is achieved when the maximum residue falls below 10^{-4}.

2.8 Boundary conditions for the 3D model

Both types of model have an inlet and different outlets. The outlets are in correspondence of the left and right iliac arteries, the right and left renal, and of the superior mesenteric artery. Boundary conditions at the entrance and exits are required to carry out the simulations. All the data used were taken from previous works (Alastruey et al, 2008, Hyun et al, 2007, N. van de Vosse, 2011, Olufsen et al, 2000, Reymond et al, 2009, Shervin et al, 2003, Vignon-Clementel et al, 2006, Xenos et al, 2019). At the inlet a velocity is always set, at the outlet different conditions are set, simulations with zero pressure and with given pressure profile have been carried out. In Figure 21 the conditions are represented in detail in case a pressure profile is

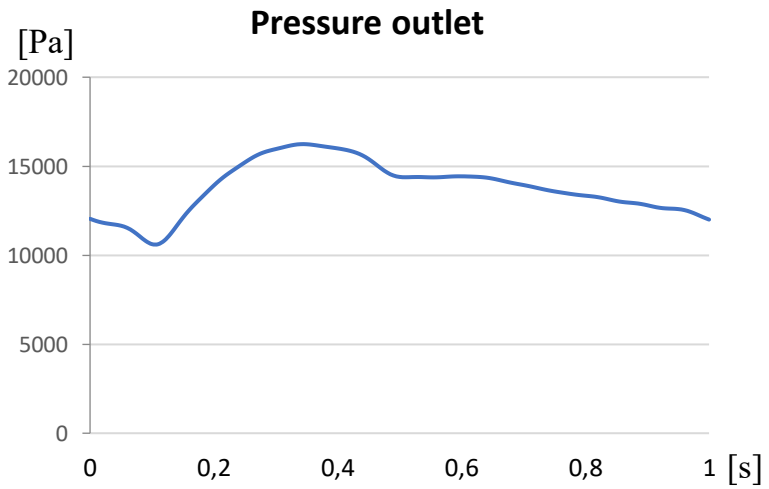

Figure 21. Outlet boundary condition rapresentation.

imposed on the outputs. In Figure 22 the inlet boundary condition is represented. In both the cases with outlet pressure = 0 and outlet pressure as a pressure profile the inlet has the same boundary condition.

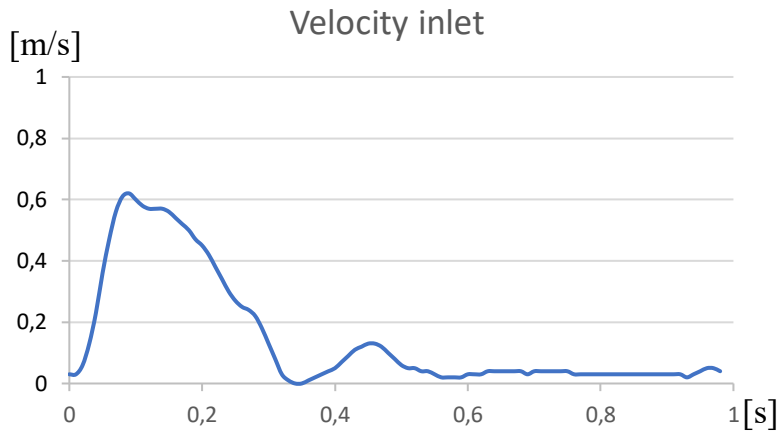

Figure 22. Inlet boundary condition.

In this work some hemodynamic descriptors have been analysed in order to study the stresses acting on the wall of the vessel. These parameters are intended to highlight areas where hemodynamics is disturbed and which could lead to the triggering of pathological situations.

The Wall Shear Stress (WSS) is defined as the tangential stress exerted by blood flow on the inner wall of the vessel (Pankaj et al, 2010). Several studies have shown that the physiological behavior of vessels is influenced by the WSS, high values of WSS can degenerate their endothelial wall. In particular, the WSS is considered an important parameter to be studied in the case of formation of atherosclerotic plaques as it can be considered a precursor due to the possibility of activating the plates through the mechanical stress (Malek et al, 1999). High values of WSS can lead to the failure of stent inplant due to the stent migration (Soudah et al, 2013).

WSS is defined by the relation

$$\tau_w = -\mu\left(\frac{\partial v_x}{\partial y}\right)_{y=R}$$

where: μ dynamic viscosity in Pa·s, y distance from the vessel wall, R is the radius of the vessel and v_x flow velocity parallel to the wall and directed along the vessel axis.

A near-wall descriptors linked to the WSS is the TAWSS, i.e. the time-averaged WSS. It is defined by the relation

$$TAWSS(s) = \frac{1}{T}\int_0^T |WSS(s,t)|dt$$

Where T is the period of the cardiac cycle, τ_w is the vector of WSS, s is a generic location of the surface.

Depending on the value assumed by TAWSS, there can be different consequences; for TAWSS less than 0.4 Pa arteriosclerosis is promoted, moreover, the aggregation of red blood cells that can lead to the formation of thrombus is favoured; if TAWSS is greater than 1.5 Pa but less than 10 Pa the vessel is protected and the condition is physiological, if TAWSS exceeds 10-15 Pa endothelial dysfunctions can be caused.

Another relevant indicator is the shear index oscillators (OSI). It is an indicator for the risk of thrombus formation, it indicates whether the WSS and the TAWSS are aligned during a cardiac cycle, if the WSS inverts his direction during the cycle. If OSI is low, (OSI<0.2) the flow is defined as unidirectional while for OSI>0.2 values the blood flow oscillates in the two directions during the cardiac cycle. This situation leads to the formation of retrograde flow and the development of endothelial dysfunctions (Xenos et al, 2019). It is defined by the relation

$$OSI(s) = 0.5\left[1 - \frac{\frac{1}{T}\left|\int_0^T WSS(s,t)\,dt\right|}{\frac{1}{T}\int_0^T |WSS(s,t)|dt}\right]$$

RRT stands for relative residence time and indicates the time the molecules spend near to the endothelium. RRT is derived from a combination of OSI and TAWSS according to the equation:

$$RRT = \frac{1}{(1-2OSI)TAWSS}$$

High RRT values can be derived from low TAWSS values or high OSI. Since the variation of RRT depends on two factors, it is often preferred to observe TAWSS and OSI individually to avoid biases.

Helicoidal structures are important within the fluid domain that is analyzed; they are greatly influenced by the geometry of the artery and affect hemodynamics, in particular by dissolving disordered structures and restoring physiological hemodynamics. Helicity is defined by the relation:

$$H(t) = \int_V \boldsymbol{v}(\boldsymbol{s},t) \cdot \boldsymbol{w}(\boldsymbol{s},t) dV$$

where $\boldsymbol{v}(\boldsymbol{s},t)$ is the velocity vector, $\boldsymbol{w}(\boldsymbol{s},t)$ is the vorticity vector and V the fluid domain volume.

The parameters of average helicity (h_1), helicity intensity (h_2) and helical flow topology normalized to volume (h_3 and h_4) are defined as

$$h_1 = \frac{1}{TV_i} \int_T \int_{V_i} \boldsymbol{v}(\boldsymbol{s},t) \cdot \boldsymbol{w}(\boldsymbol{s},t) dV\, dt$$

$$h_2 = \frac{1}{TV_i} \int_T \int_{V_i} |\boldsymbol{v}(\boldsymbol{s},t) \cdot \boldsymbol{w}(\boldsymbol{s},t)| dV\, dt$$

$$h_3 = \frac{h_1}{h_2}$$

$$h_4 = \frac{|h_1|}{h_2}$$

h_1 is the helicity averaged along the cardiac cycle, h_2 represents the intensity of the helicity averaged along the cardiac cycle and in the volume; h_3 can assume different values between $-1 < h_3 < 1$, $h_3 = -1$ in case left-handed helical structures are in

the fluid domain, while it assumes positive unit value when the prevalent helical structures are right-handed. h_4 is the magnitude of h_3 and indicates the intensity of the rotation of the fluid domain structures, h_4 does not analyze the direction and direction of rotation. In order to represent the helical structures of the fluid domain, a parameter called Local Normalized Helicity (LNH) defined by the relation is used:

$$LNH = \frac{\boldsymbol{v}(\boldsymbol{s},t)\cdot\boldsymbol{w}(\boldsymbol{s},t)}{|\boldsymbol{v}(\boldsymbol{s},t)\cdot\boldsymbol{w}(\boldsymbol{s},t)|} = \cos\varphi,$$

where φ is the angle between vectors velocity and vorticity vectors. LNH values range between -1 and 1; the extremity values indicate a purely helical flow, and zero value represent the presence of reflectional symmetry in the flow (Tittel et al., Anatomia funzionale dell'uomo). LNH sign is an indicator of the direction of rotation of helical structures in the fluid domain that could be left or right-handed respectively if the sign is – or +. Helical flow has a key role in suppressing flow disturbances as shown elsewhere. LNH is an indicator related to bulk flow, it is used because it analyses a helical flow, which is of fundamental importance in dissolving disturbed flows. In addition, low velocity vortical zones are dangerous because they favour thrombi formation.

During the realization phase of the model, the renal arteries and the mesenteric artery were reconstructed also inside the main lumen. In order to ensure the passage of blood inside the renal, mesenteric and iliac arteries and in order to quantify and compare the amount of fluid flowing inside them both before and after the operation, a study is made on the flow rate out of the arteries. For each outlet, the mass flow rate is computed, the results are displayed by making a percentage of the flow rate coming out of the arteries compared to the inlet flow rate according to the example report on the right kidney:

$$Q_{m,rightrenal}\% = \frac{Q_{m,righ\_trenal}}{Q_{m,inlet}}$$

3 Results

The following is an illustration of the results for the unsteady-state fluid dynamics simulations performed. The results have been calculated for the models of the two patients, both in pre- and post-operative conditions, and simulations with different boundary conditions have been carried out for each model: in inlet a velocity profile is always imposed while in outlet: (1) once a pressure waveform is imposed and (2) once a pressure equal to zero.

3.1 Cardiac cycle averaged descriptors

The values referred to near wall descriptors of average quantities such as Oscillatory Shear Index (OSI), Time Averaged Wall Shear Stress (TAWSS) and Relative residence Time (RRT) are initially reported; these indicators are important as they describe the overall hemodynamic trend of the cardiac cycle; a variation of them provides information on the differences between pre-operative and post-operative cases. Subsequently, pressure and Wall Shear Stress (WSS) are studied for significant instants of the cardiac cycle, in particular systole, deceleration and diastole.

The trend of TAWSS for all cases is reported in the following rapresentations, the cases obtained with the different boundary conditions are compared.

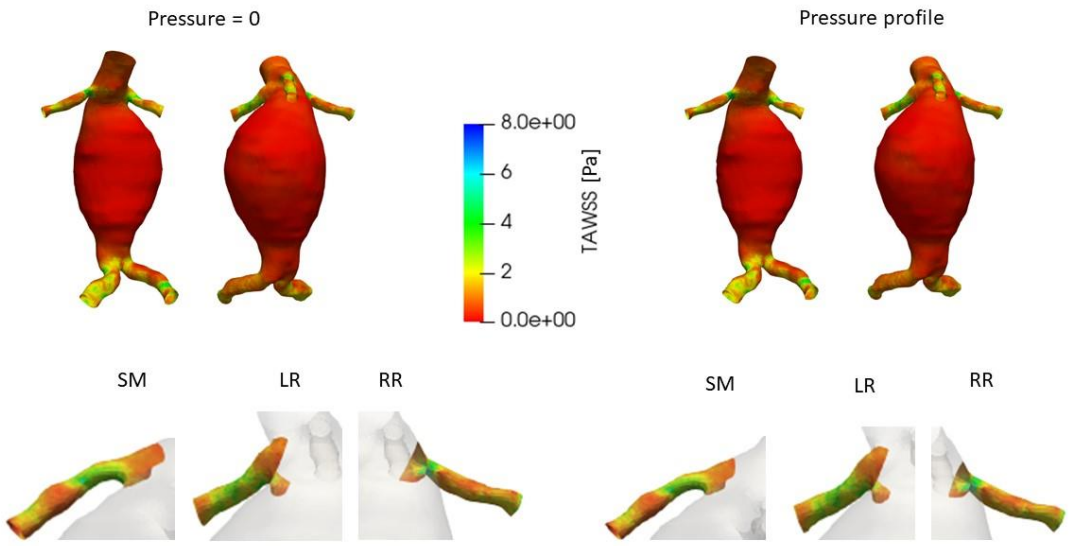

Figure 23. TAWSS trend patient NT pre operative.

In the pre-operative case, for the NT patient, the TAWSS for outlet pressure given by a profile or zero outlet pressure does not show significant differences, a visual analysis shows a very low and uniform TAWSS value close to the aneurysmatic area which suggests, for TAWSS below 0.4 Pa the risk of atherosclerosis and thrombus formation by aggregation of red blood cells. In the area close to the renal arteries, and in particular in the transition from large arteries to small arteries, TAWSS values are greater, it can be seen they have TAWSS within the range 1.5 Pa < TAWSS < 4.5 Pa, because the physiological range is 1.5 Pa < TAWSS < 8 Pa the vessel wall is protected both from the risk of aggregation of blood cells and the risk of degeneration of endothelium caused by over the range TAWSS.

In Figures 24 the TAWSS trend is reported for the PE patient, close to the aneurysmatic area the time-averaged WSS is higher than the NT patient, for PE there are TAWSS values higher that 0.4 Pa but not in the physiological range. Even in the case of the PE patient, close to the transition from large and small arteries, greater TAWSS values than those of the main lumen are found.

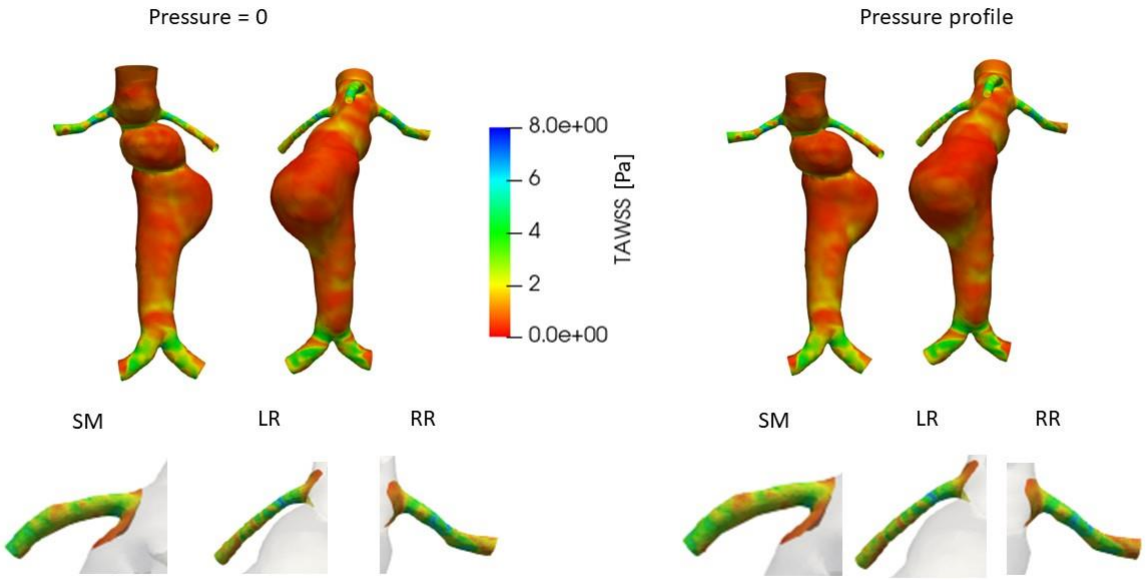

Figure 24. TAWSS trend patient PE pre operative.

In Figure 25 and Figure 26 the results of TAWSS for the two patients in the post-operative case are shown. In both cases there is an increase in TAWSS values in the abdominal area previously affected by the aneurysm, which was previously characterized by a very low TAWSS with disturbed hemodynamics. After the surgery TAWSS values are over the minimum physiological value of 1.5 Pa.

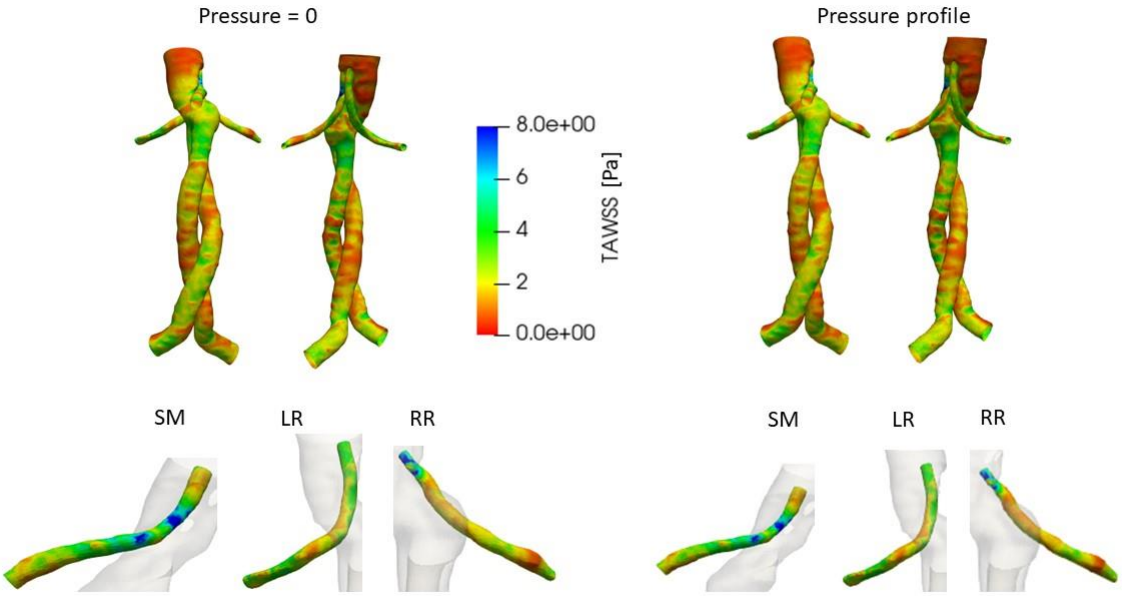

Figure 25. TAWSS trend patient NT post operative.

For NT patients post operative, TAWSS values in the proximity of secondary arteries (renal and mesenteric arteries) are in the range 1.5 Pa < TAWSS < 8 Pa, in particular there are points where TAWSS values > 8 Pa are found. Since they are localized points and do not affect a large area of the surface, it can be thought that they are high TAWSS points due to the geometry and in particular to the model reconstruction, therefore they are not to be considered dangerous in the analysis.

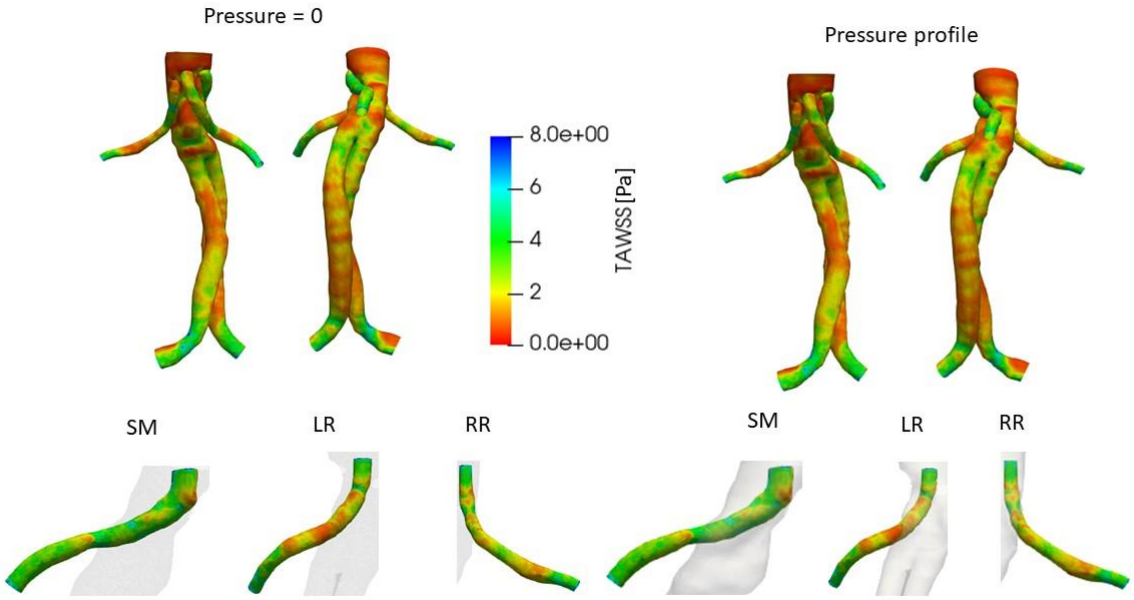

Figure 26. TAWSS trend patient PE post operative.

As shown in Figures 26 the TAWSS values for the PE patient after surgery in the renal and mesenteric arteries are in the range 1.5 Pa < TAWSS < 6 Pa.

In both patients, both pre- and post-operatively, there are no noteworthy differences for the two pressure boundary conditions at the outlets.

Another parameter observed during the study phase of the results is the Oscillatory Shear Index (OSI) which specifies how much the flow reverses its direction during the cardiac cycle. This is also an average value referring to the cardiac cycle and not to the single instant.

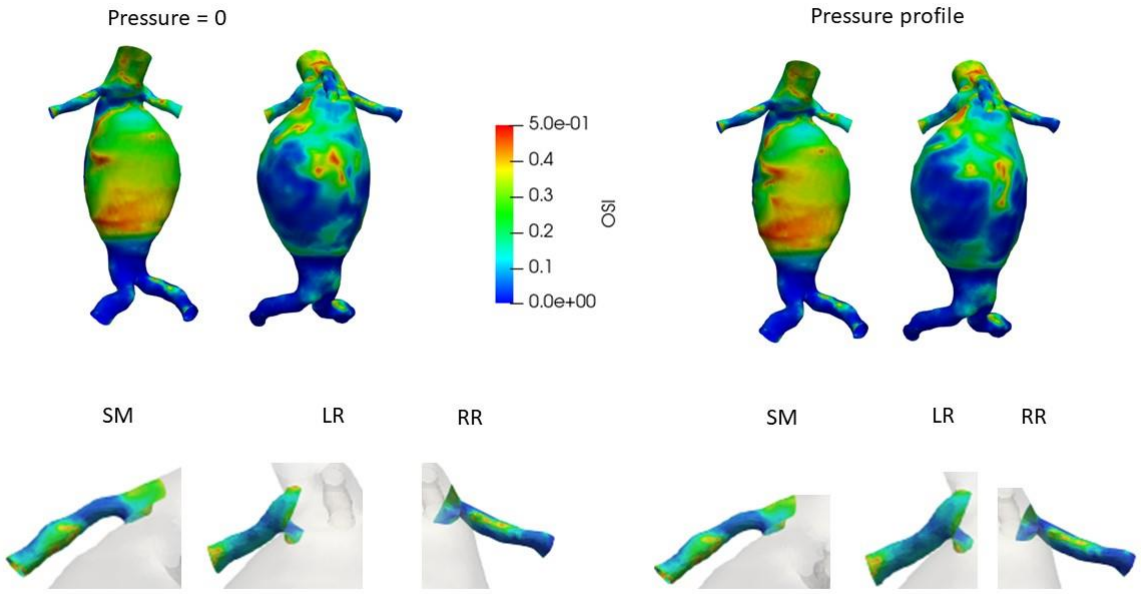

Figure 27. OSI trend patient NT pre operative.

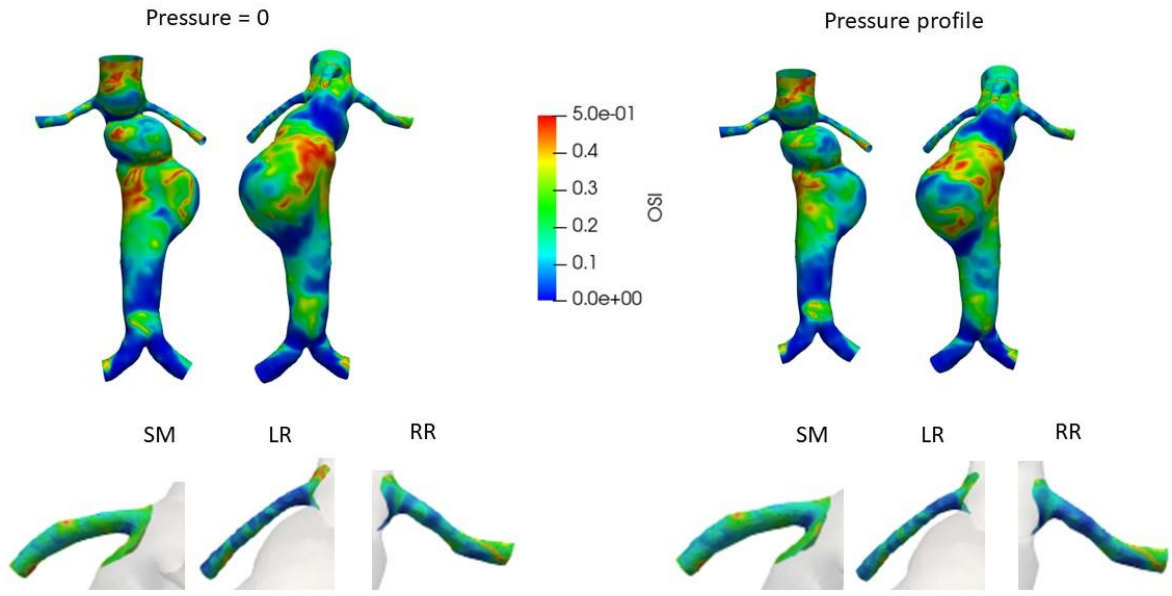

Figure 28. OSI trend patient PE pre operative.

In the pre-operative case in both patients there is no difference between the two pressure boundary conditions imposed. For both patients studied, in pre-operative condition areas with high OSI are observed close to the aneurysmatic area where $0.2 < OSI < 0.5$. In the close proximity of the iliac arteries the OSI values are close to zero, from which it can be deduced that in the iliac arteries the flow does not reverse its direction and the hemodynamics that is created are not disturbed. The renal and mesenteric arteries have values of low OSI ($OSI < 0.2$) so the flow is unidirectional as in the iliac.
Below is the OSI trend following the stent graft insertion operation.

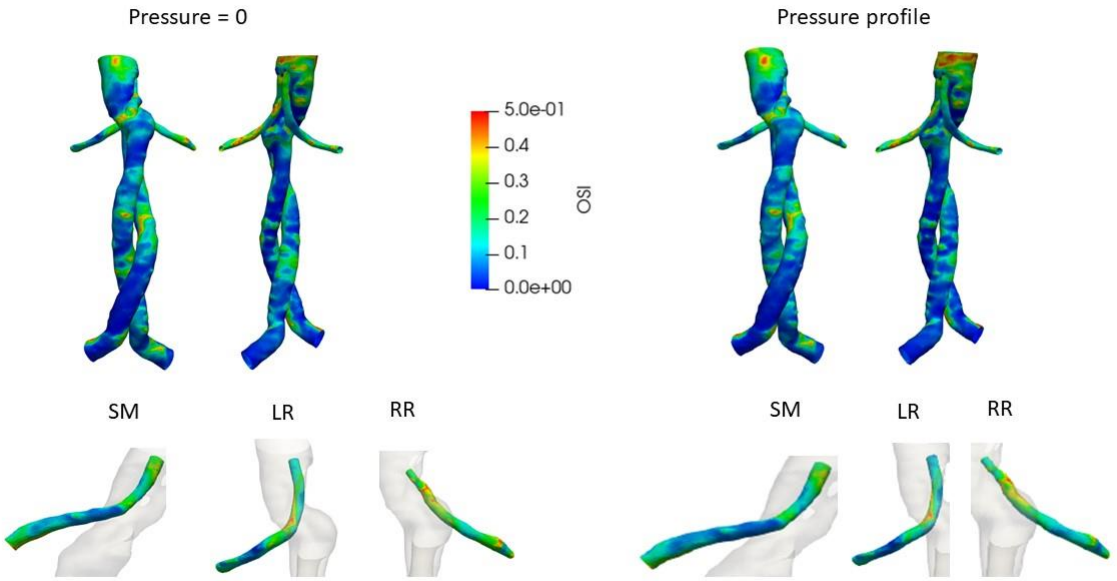

Figure 29. OSI trend patient NT post operative.

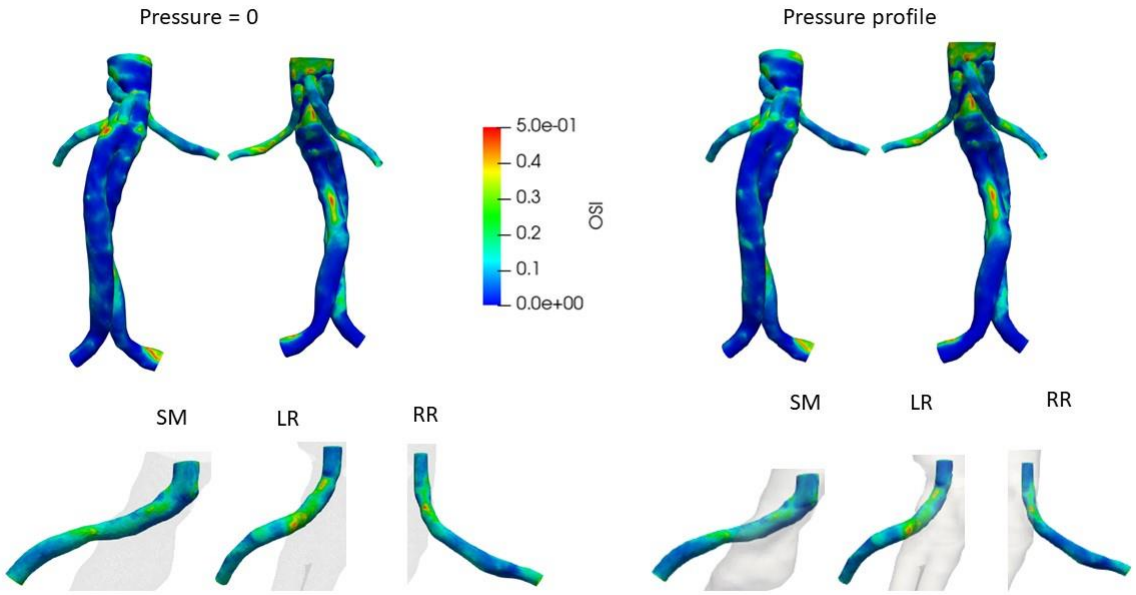

Figure 30. OSI trend patient PE post operative.

In post-operative cases OSI shows a decrease in the area previously affected by the aneurysm where OSI values are now less than 0.2. In the main lumen there are small isolated areas with high OSI, these could be re-construction errors. The OSI values in the renal and mesenteric arteries do not show a change. Based on these results it can be said that after the operation the flow is much more mono-directional than in the pre-operative phase.

A trend similar to the OSI can be found in Relative Residence Time (RRT) that shows how long molecules spend near the endothelium. RRT is influenced by OSI and TAWSS but the TAWSS component is less incisive than the OSI component. The following images show the models and their color maps related to RRT.

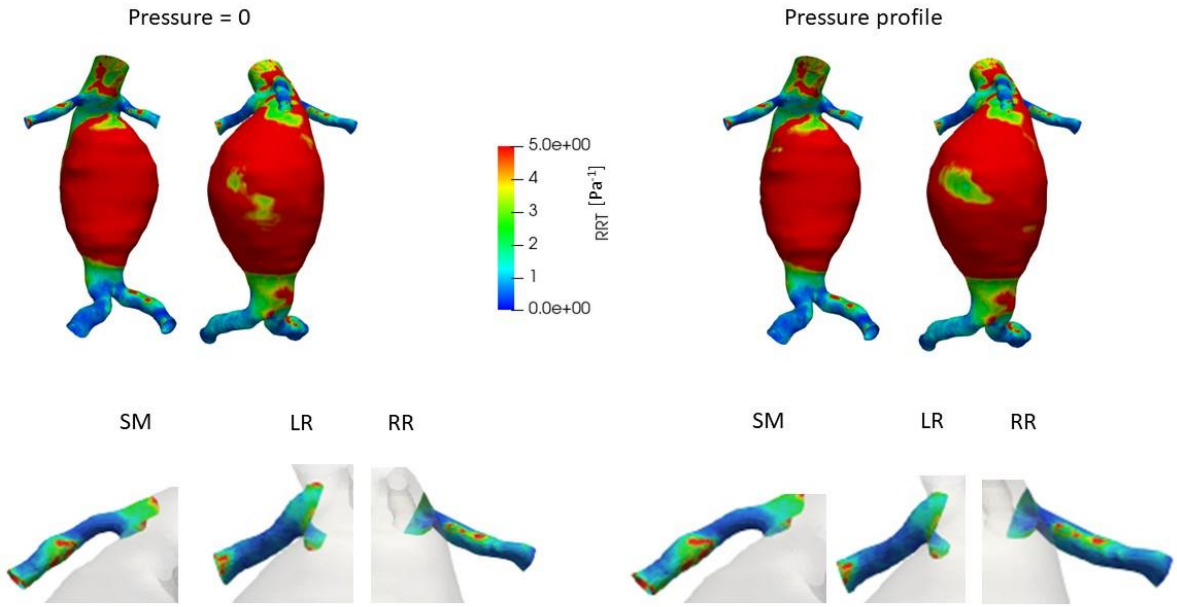

Figure 31. RRT trend patient NT pre operative

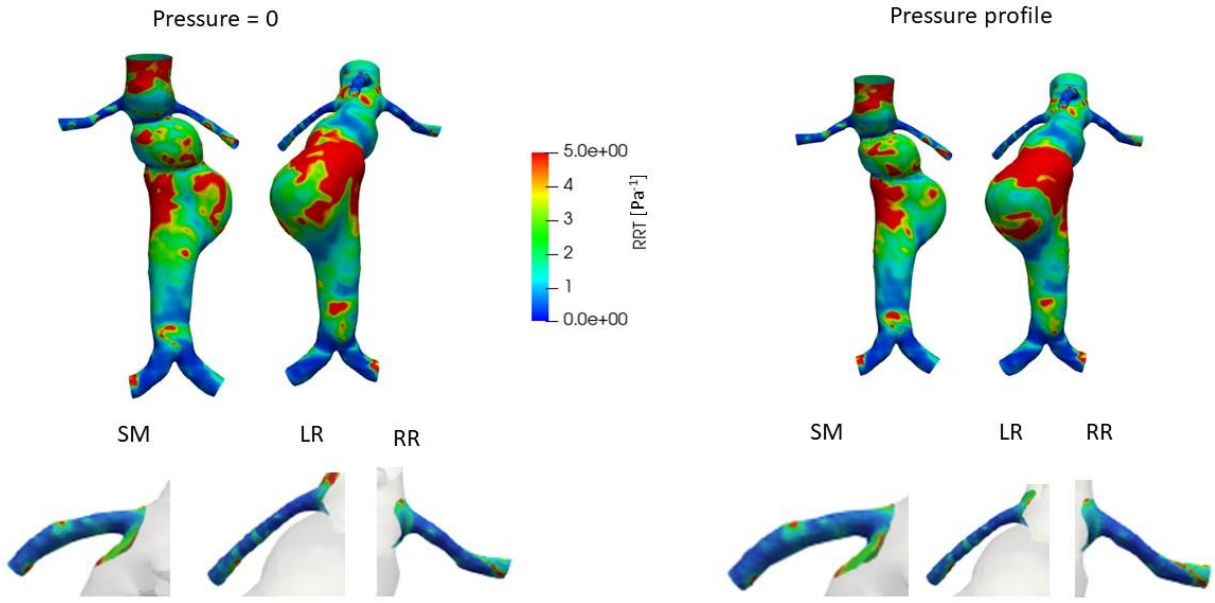

Figure 32. RRT trend patient PE pre operative.

In the pre-operative case there is a high RRT in the aneurysmatic area which indicates high cell residence time on the wall endothelium, this can lead to cell aggregation. This

behaviour is highly observable for the NT patient. Renal, mesenteric and iliac arteries show a low RRT profile.

In post-operative cases the RRT pattern is observable in Figure 33 and Figure 34.

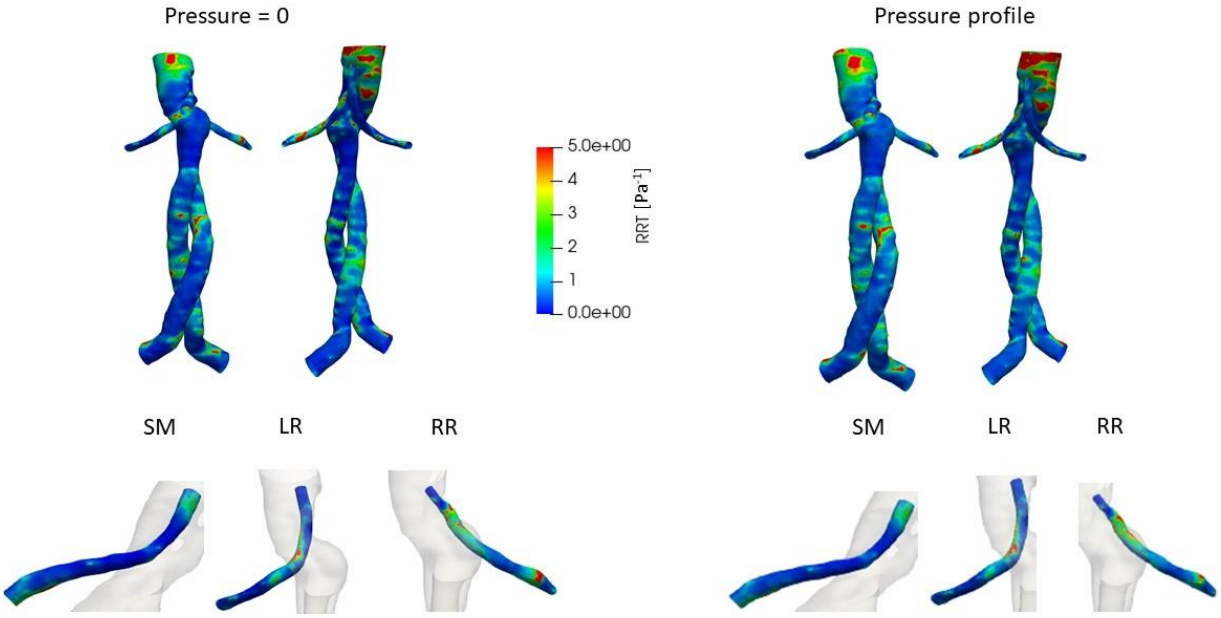

Figure 33. RRT trend patient NT pre operative.

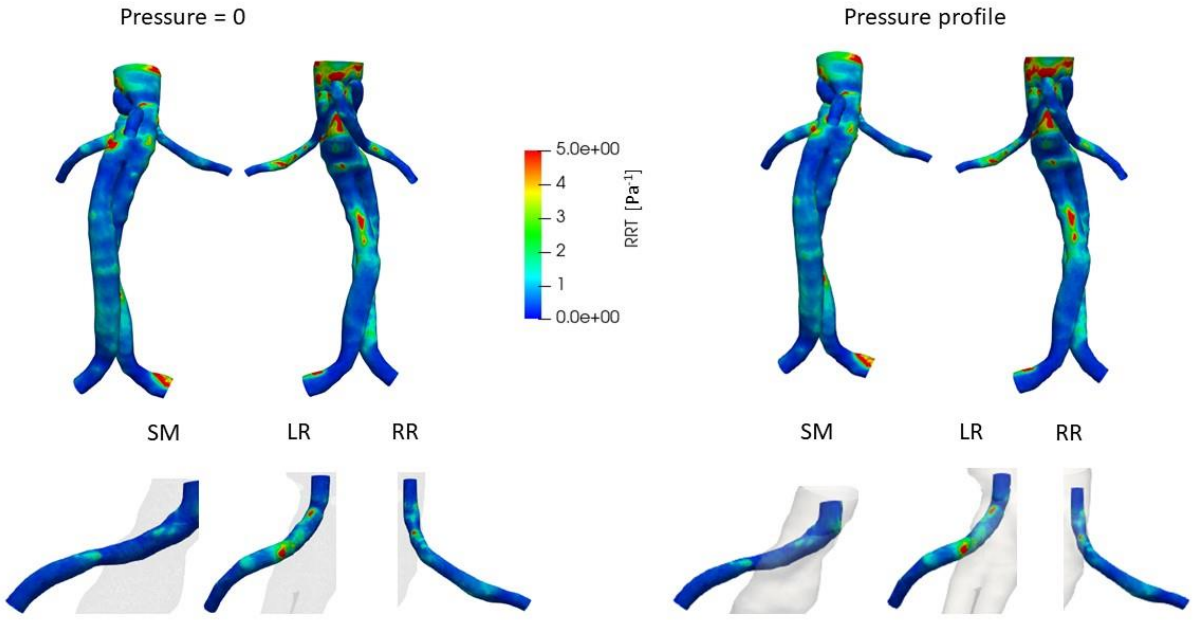

Figure 34. RRT trend patient PE post operative.

In the post-operative case the RRT values decrease, areas with maximum RRT value of 5 Pa^{-1} in the main lumen are noticed and may be due to geometric reconstruction. Secondary arteries show low RRT values. Even in the post-operative case the RRT values are influenced by the OSI trend.

Another parameter mediated in the cardiac cycle that is analyzed is the helical flow, this is investigated by visualizing isosurfaces of LNH averaged over the cardiac cycle. LNH is analyzed for values of ±2, where +2 (red) corresponds to a right-handed helical rotation and -2 (blue) to a left-handed helical rotation. As can be seen in the following representations, within the analyzed models there is an equilibrium situation, there are no great differences between the two boundary conditions imposed on the output.

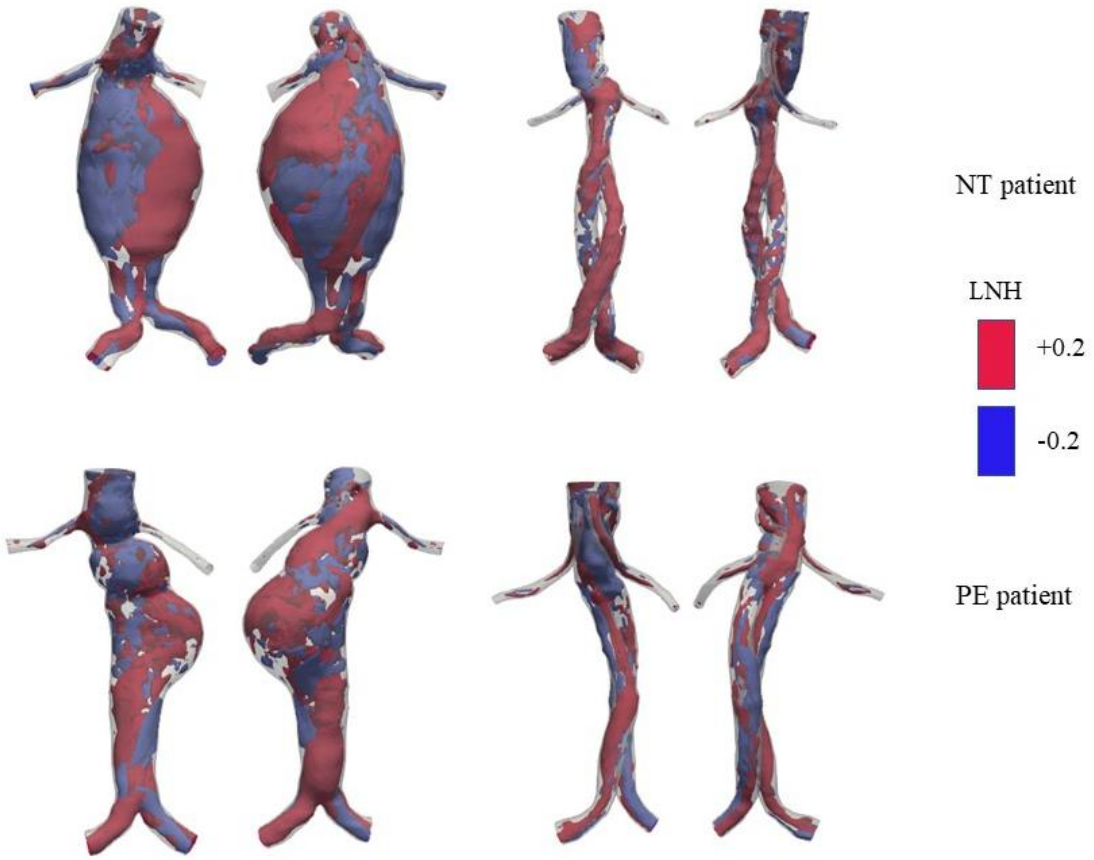

Figure 35. Cycle-averaged LNH, positive LNH right-handed helical rotation, negative LNH left-handed helical rotation.

3.2 Wall shear stress and Pressure anlysis

After analyzing the mean quantities, the Wall Shear Stress (WSS) and pressure, especially for systole, deceleration and diastole, are analyzed. These quantities are investigated for both conditions at the outlet for both patients and the results are shown below.

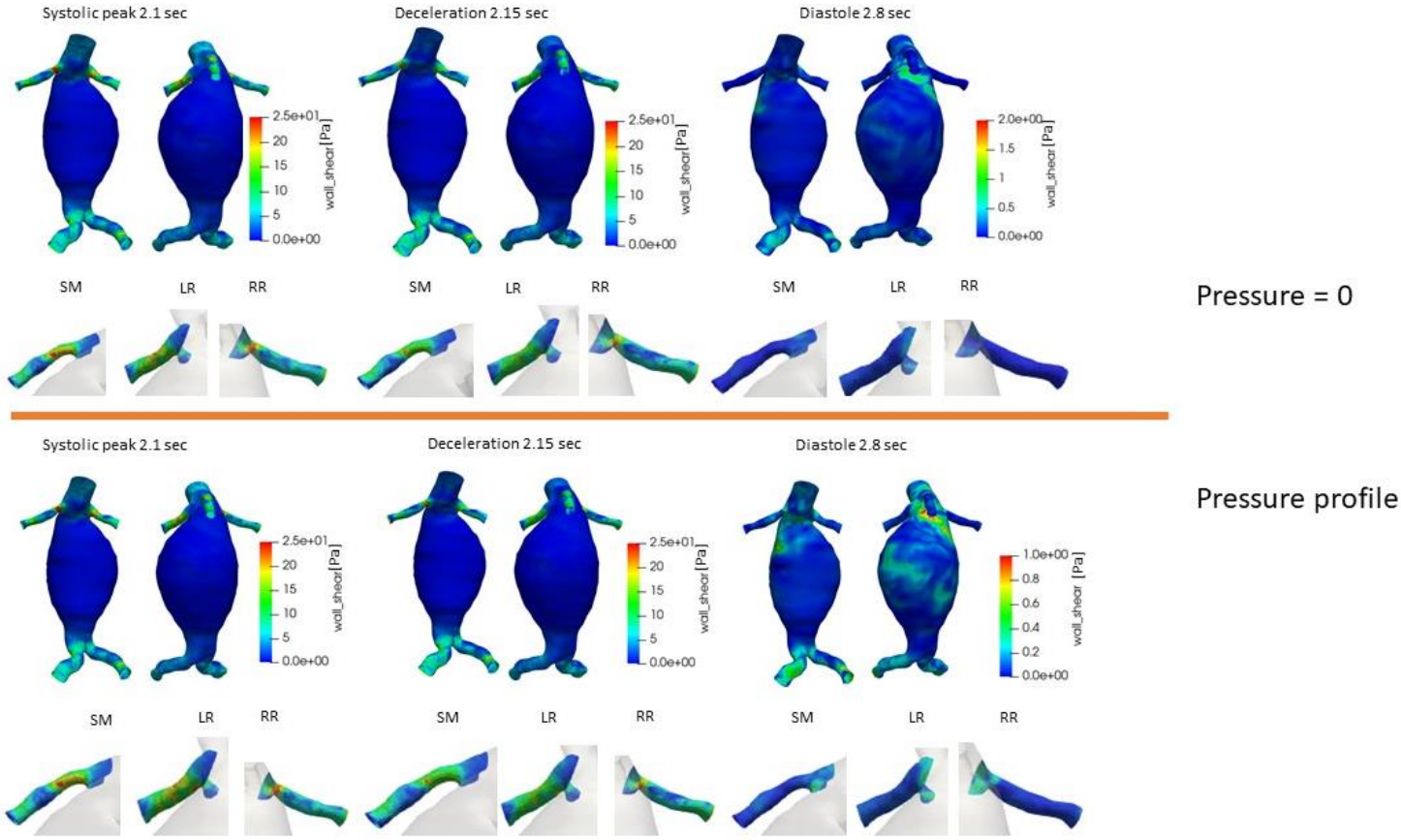

Figure 36. Wall Shear Stress trend patient NT pre operative in systole, deceleration and diastole.

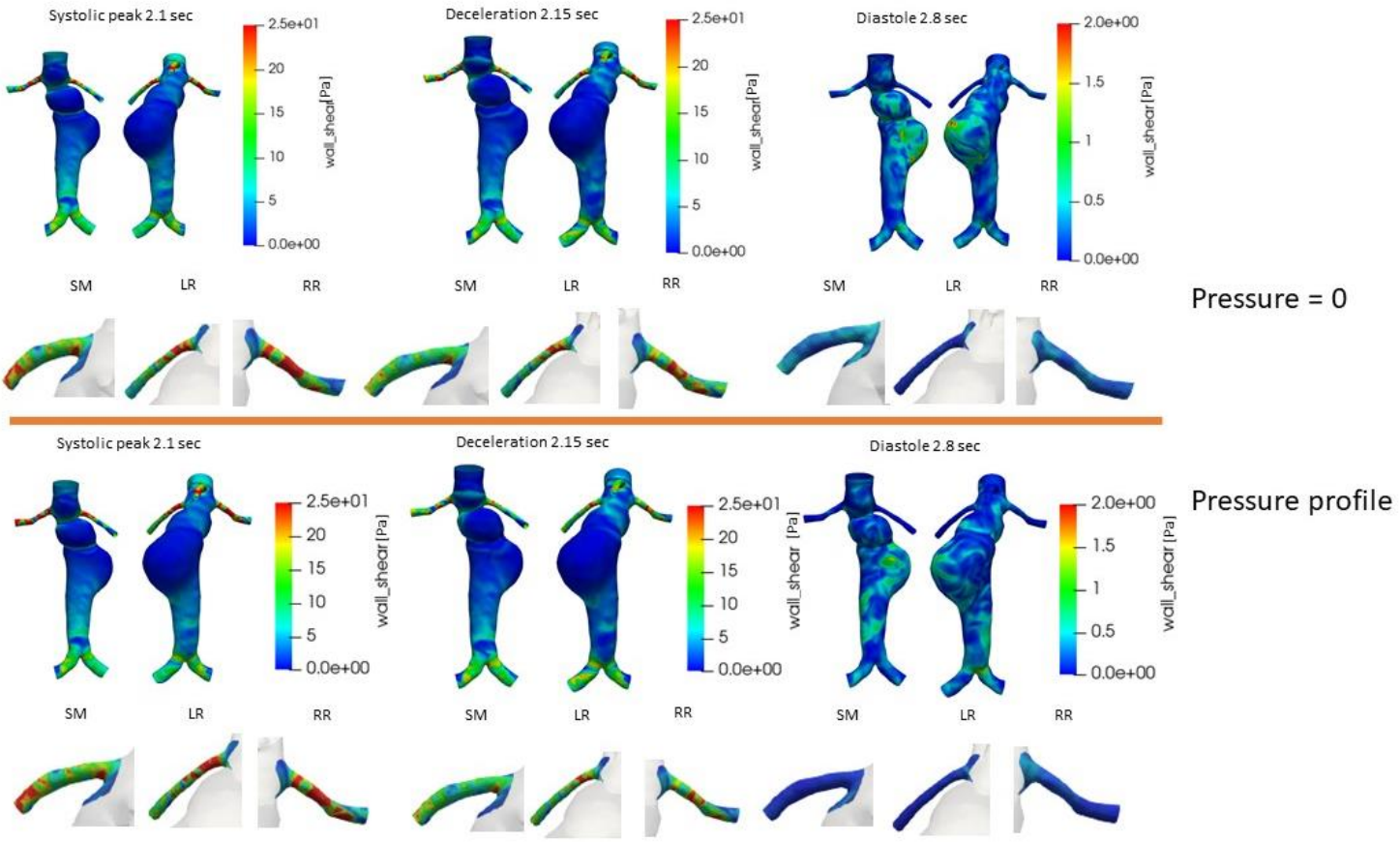

Figure 37. Wall Shear Stress trend patient NT pre operative in systole, deceleration and diastole.

In the pre-operative case, low WSS values can be observed in both patients close to the area affected by the aneurysm; low WSS values are significant in recirculation areas, which are dangerous because they promote the risk of thrombus formation. In the proximity of secondary arteries, WSS values are higher than those of the main lumen, some areas have high WSS. High WSS values can lead to damage to the endothelial wall in the pre-operative case. During the three instants of the cardiac cycle analyzed, moving from systole to diastole, an expected decrease in WSS due to the cardiac pumping action is noticeable. For the two imposed outlet conditions, no differences in the WSS results are observed for the pre-operative situation.

Figures 38 and Figure 39 show the results for WSS in the three instants of the cardiac cycle considered for the models realized on the scans referred to post-operative cases.

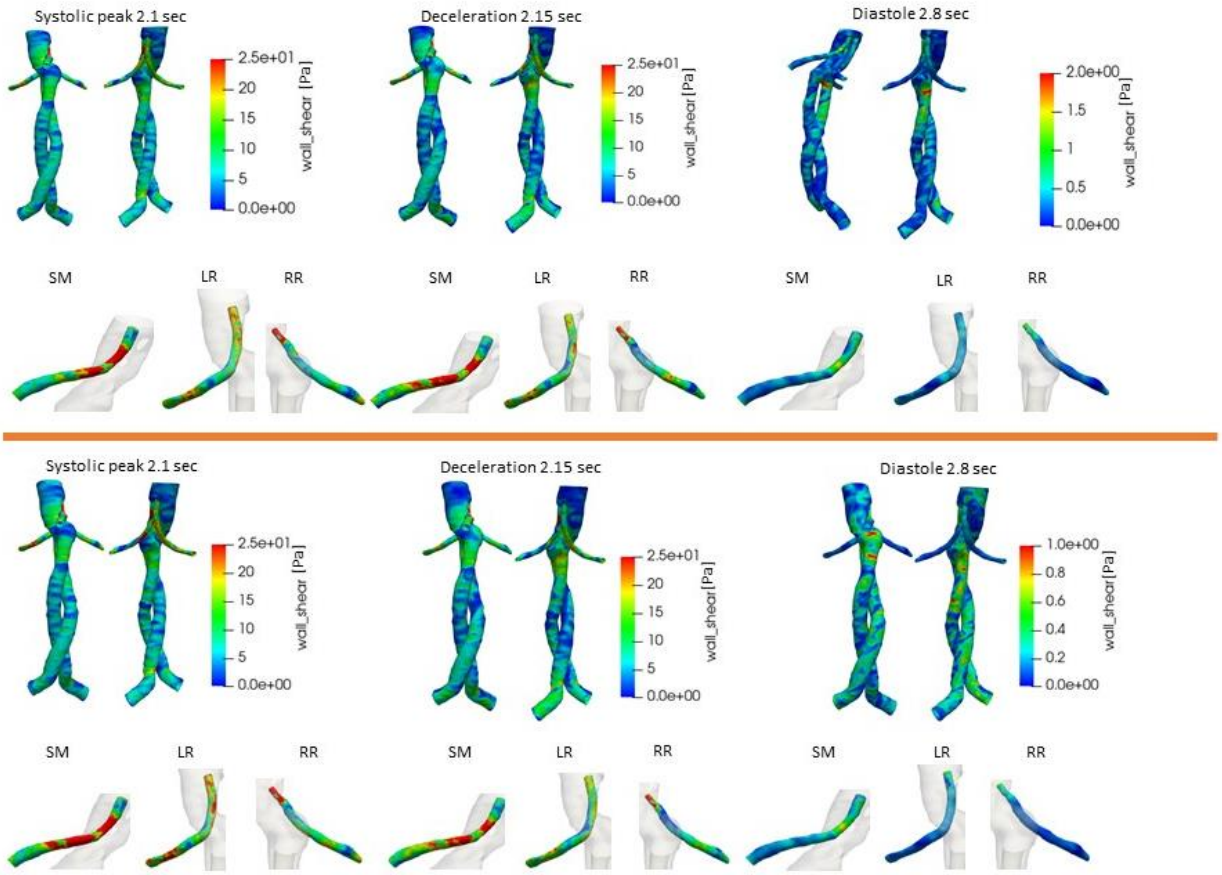

Figure 38. Wall Shear Stress trend patient NT post operative in systole, deceleration and diastole.

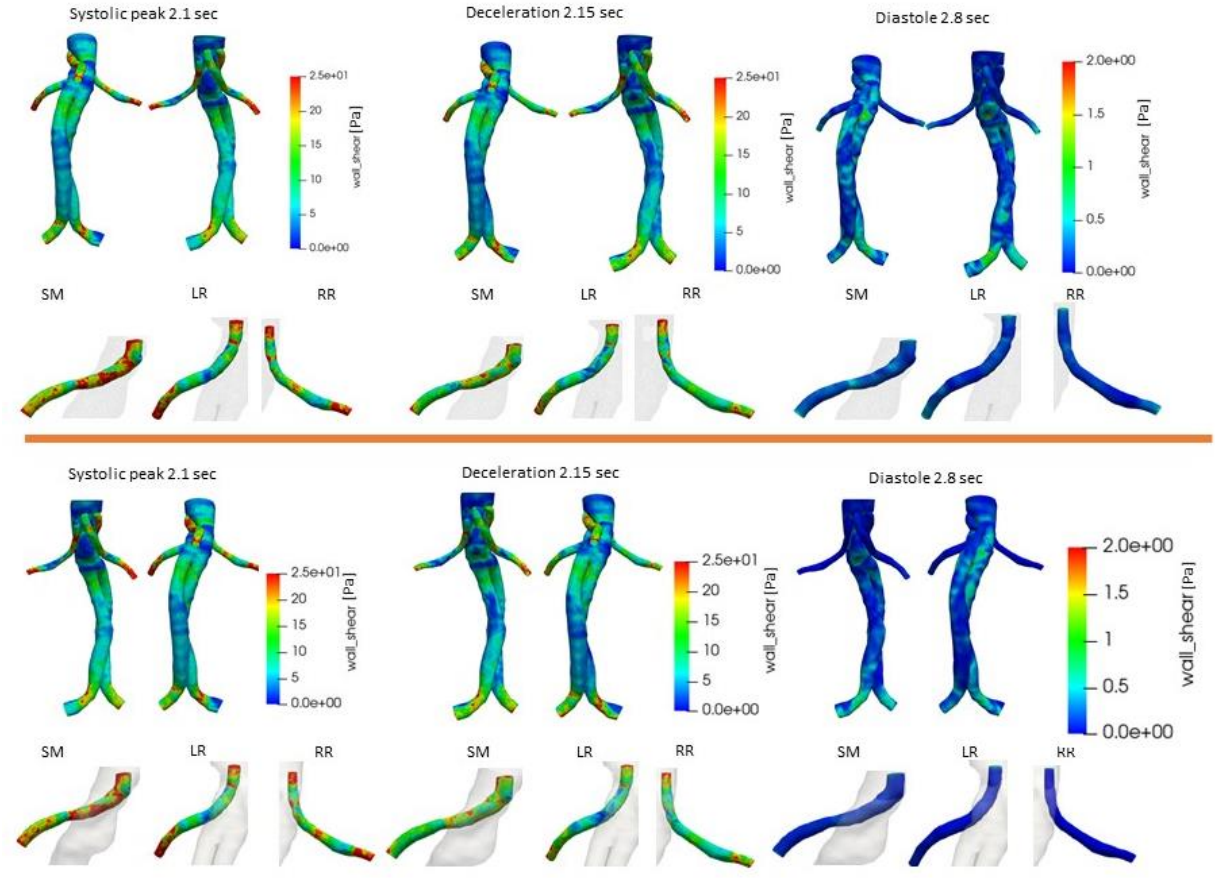

Figure 39. Wall Shear Stress trend patient PE post operative in systole, deceleration and diastole.

Observing the post-operative results there is a significant decrease in the area previously affected by the aneurysm, after the surgery the main lumen is not affected by low WSS areas. Both patients notice higher WSS values close to the iliac, renal and mesenteric arteries; these areas may be subject to the risk of stent graft migration as a result of the operation. There are high WSS points, these areas may present such high values due to the reconstruction and segmentation performed. Even in the post-operative case there are no substantial differences between simulations performed with outlet pressure profile or zero outlet pressure. During the cardiac cycle, moving from systole to diastole, the WSS decreases throughout the model.

Pressure is the parameter that is most affected by the two different pressure conditions imposed in outlet; pressure is also analyzed in both pre- and post-operative cases, in the three significant moments of the cardiac cycle; systole, deceleration and diastole.

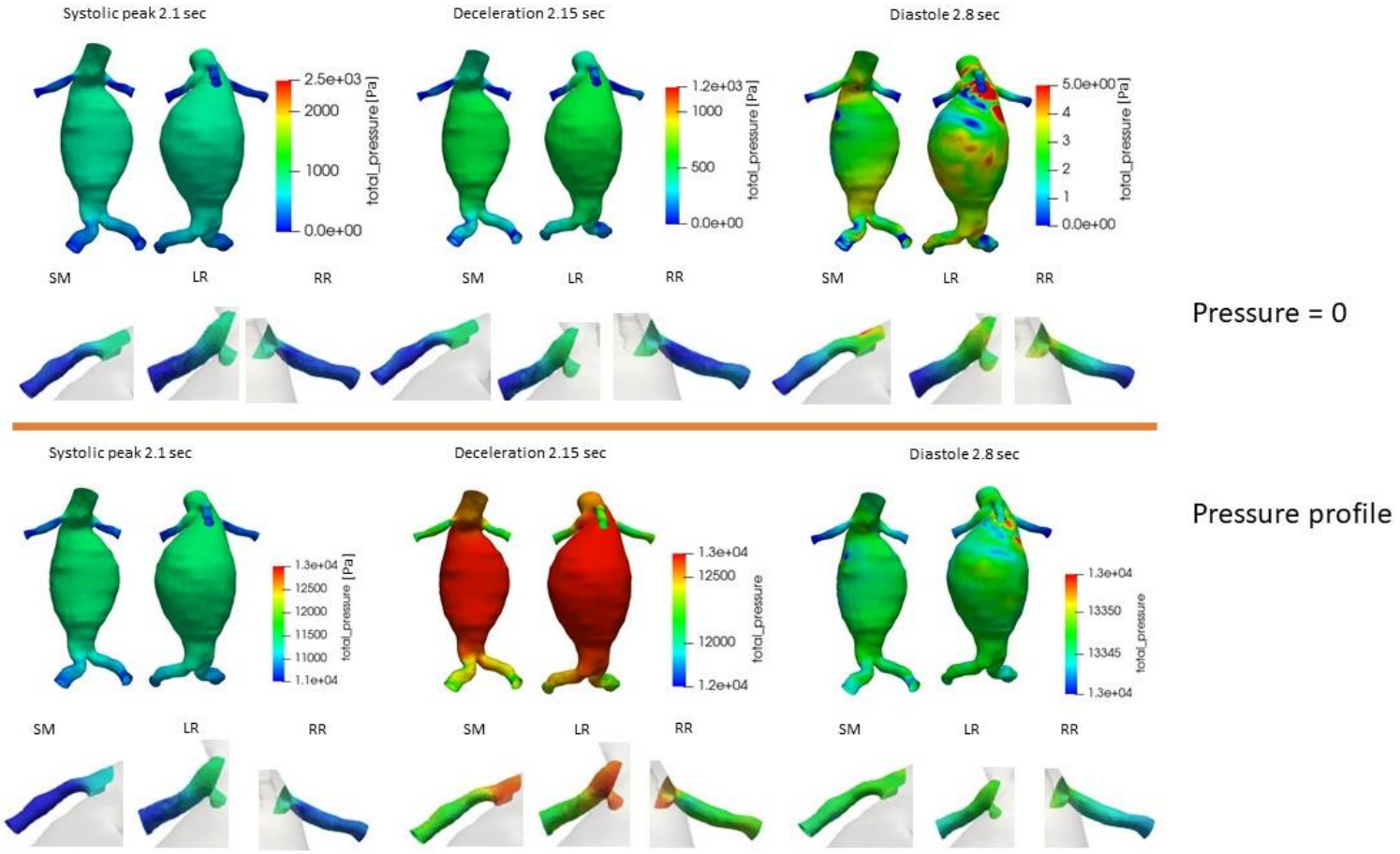

Figure 40. Pressure trend patient NT pre operative in systole, deceleration and diastole.

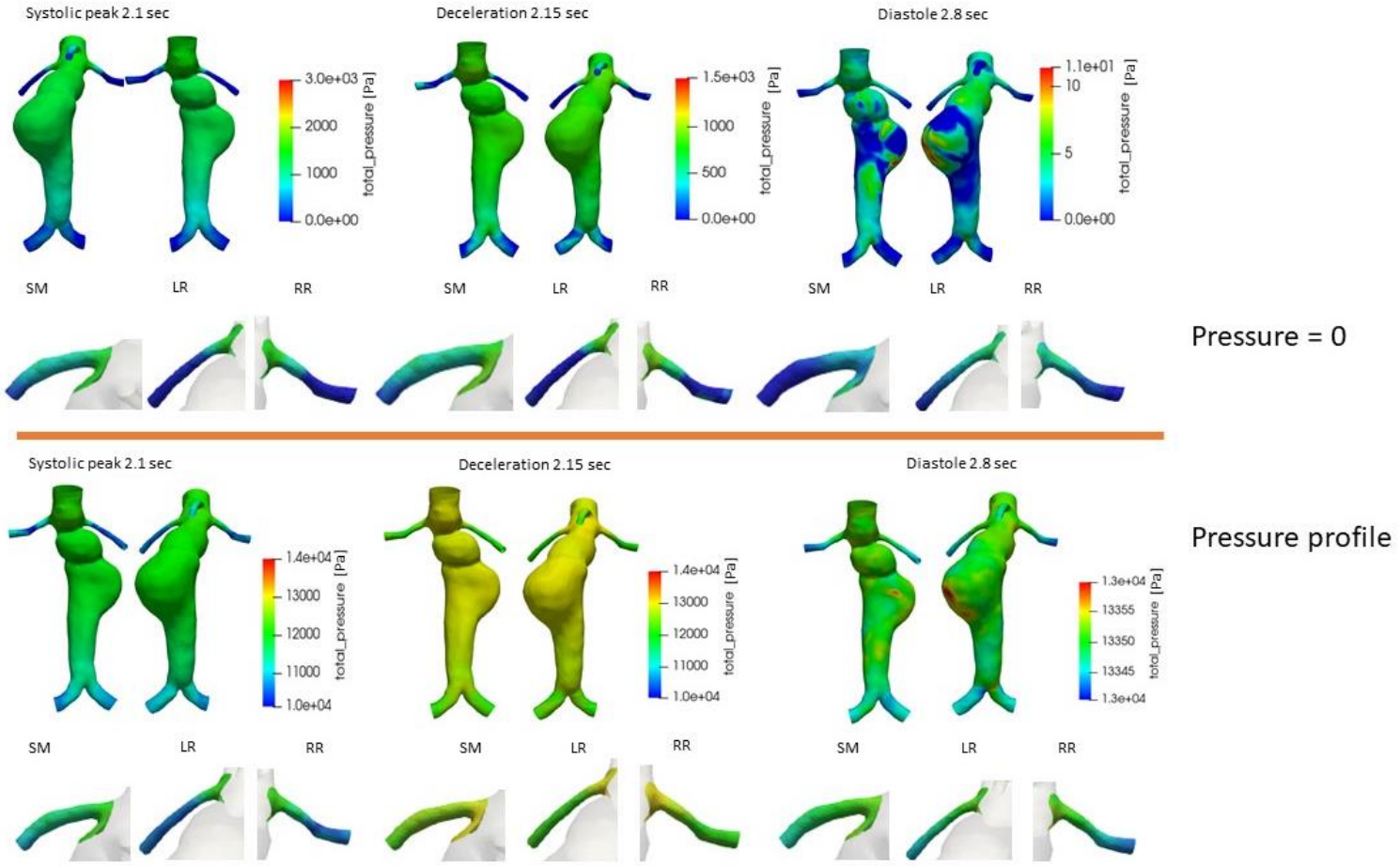

Figure 41. Pressure trend patient PE pre operative in systole, deceleration and diastole.

Figures 40 and Figure 41 show the pressure trends for the pre-operative cases for the two patients. For outlet pressure equal to zero the pressure values in the model are homogeneous and there are no large pressure drops. In the proximity of the iliac arteries and the mesenteric and renal arteries the pressure assumes low values. In the post-operative cases shown in Figures 42 and Figure 43 there is a pressure drop from proximal to distal position both in case of zero outlet pressure and in case of outlet pressure profile. Although the trend may seem similar, the minimum pressure value found in the case of outlet pressure profile should be noticed; in fact, in this case, high pressure values are maintained for both patients, while in the case of zero outlet pressure the minimum value reported was zero.

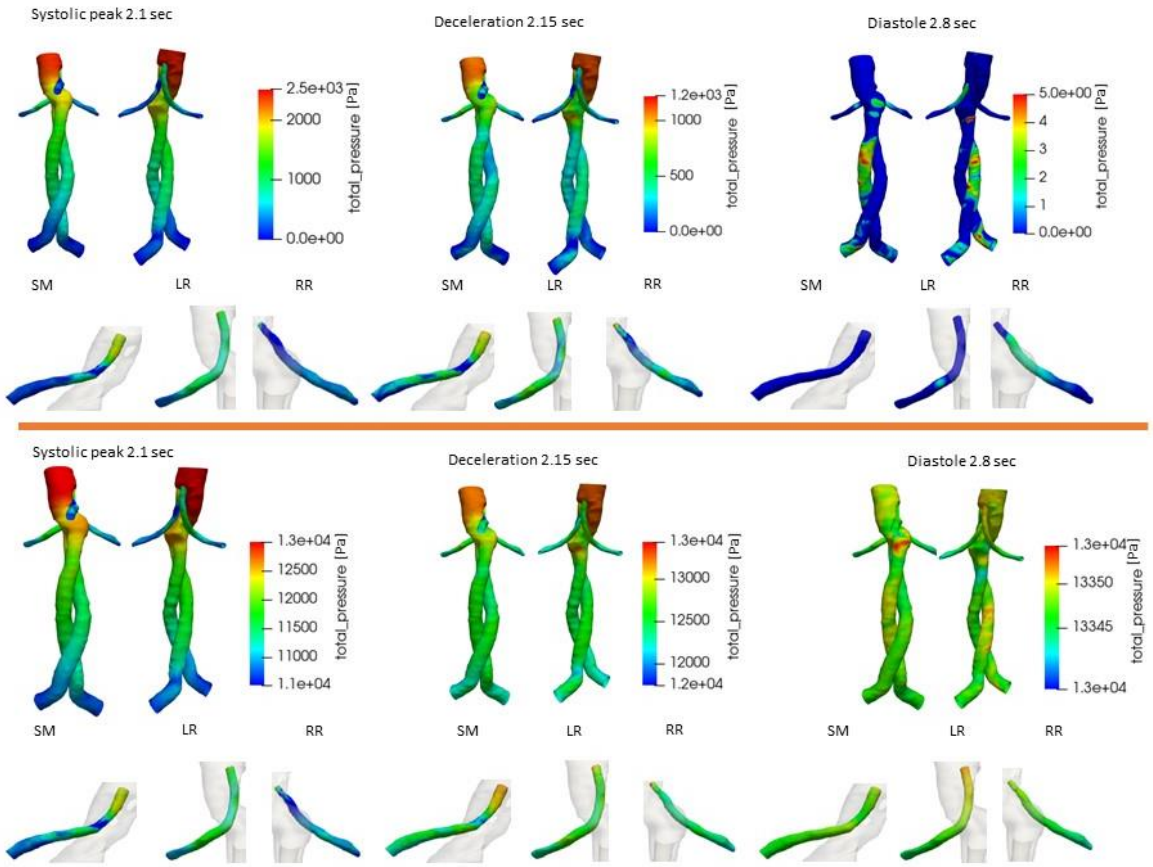

Figure 42. Pressure trend patient NT post operative in systole, deceleration and diastole.

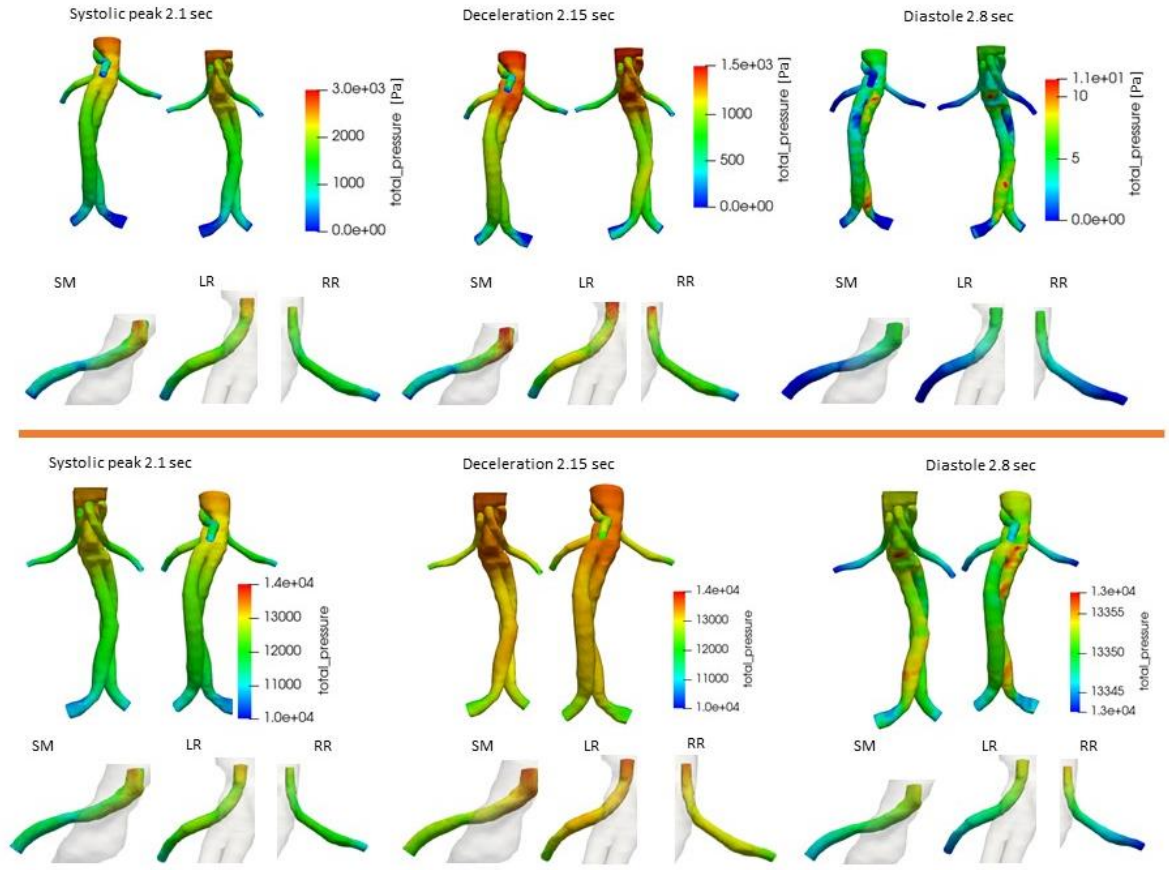

Figure 43. Pressure trend patient PE post operative in systole, deceleration and diastole.

For all cases pressure drops are also analyzed, for systole, deceleration and diastole instants pressure drops are homogeneous for profile pressure outlet and zero pressure outlet condition. The pre-operative case, as evidenced by pressure trends, has lower pressure drops than the post-operative ones, for systole the pre-operative pressure drop is about 1700 Pa while in the post-operative case it rises to 2300 Pa. For deceleration and diastole the pressure drop values decrease. Following there is a numerical analysis of pressure drop.

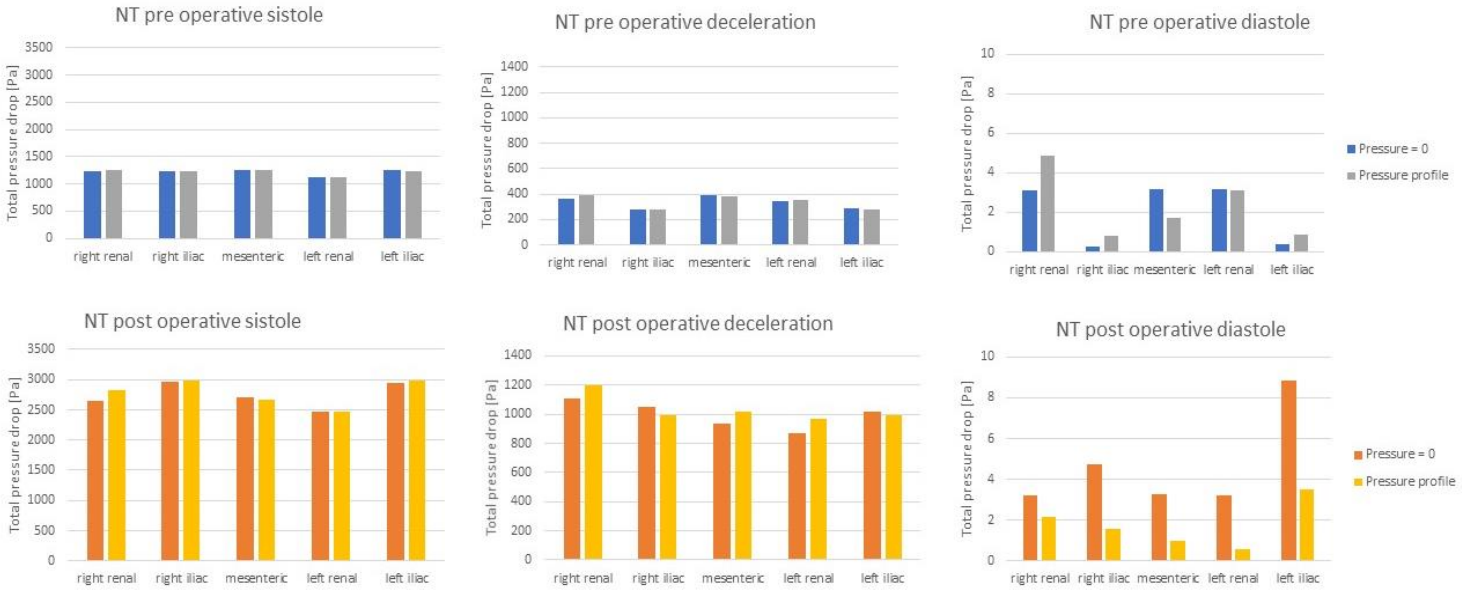

Figure 44. Pressure drop patient NT.

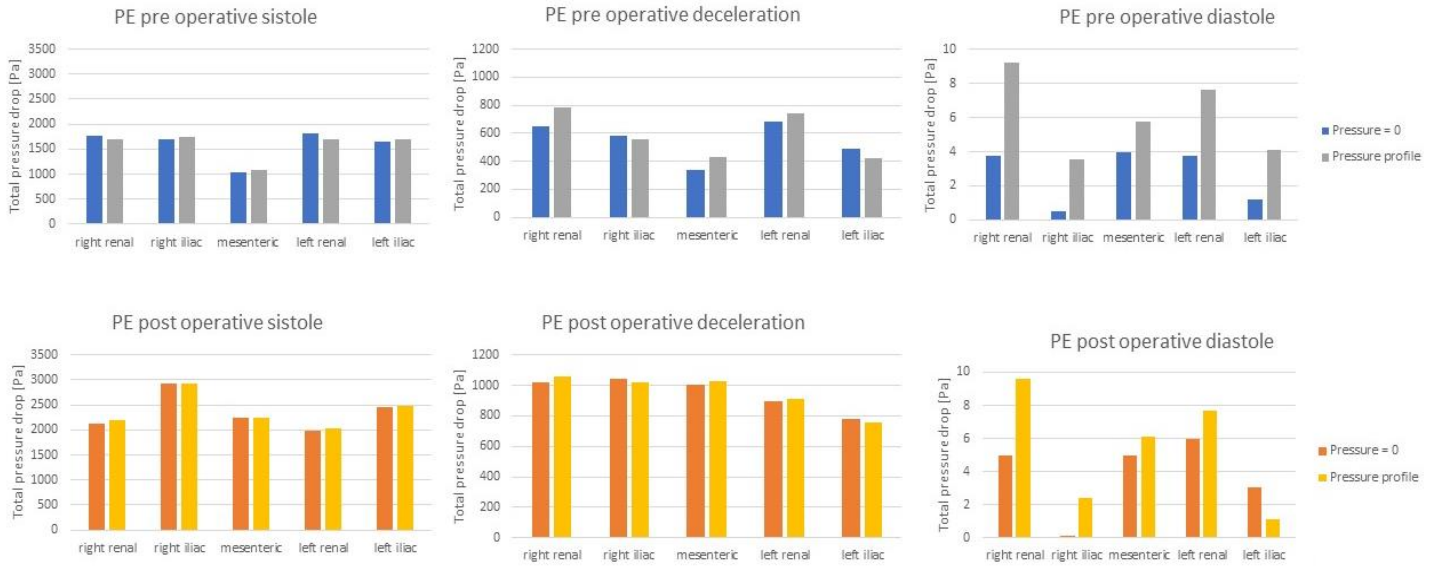

Figure 45. Pressure drop patient PE.

Following the reconstruction of the patients' geometry, especially for post-operative cases, it was important to verify that the secondary arteries, where the outlets are located, were open and that blood could flow inside them. In order to carry out this test, the percentage flow rates in outlets were calculated with respect to the inlet flow rate; in the following tables the flow rate percentages for the two patients for both the outlet pressure boundary conditions imposed can be observed.

% Flow rate - Zero pressure outlet condition					
% PE pre	**right renal**	**left renal**	**mesenteric**	**right iliac**	**left iliac**
sistole	-11,25472952	-6,35205444	-10,79222565	-35,06431957	-36,5367926
deceleration	-9,571986407	-6,231639209	-9,104723766	-34,67389861	-40,41781233
diastole	7,038153418	0,944856041	10,80754426	-52,3480835	-66,44342472

% Flow rate - Zero pressure outlet condition					
% PE post	**right renal**	**left renal**	**mesenteric**	**right iliac**	**left iliac**
sistole	-7,291948602	-10,89860246	-16,27982929	-34,17576724	-31,35388977
deceleration	-5,750225956	-8,92912216	-13,44464555	-37,93667923	-33,93933616
diastole	3,54902945	6,442318662	9,841930928	-64,54270322	-55,28906963

% Flow rate - Zero pressure outlet condition					
% NT pre	**right renal**	**left renal**	**mesenteric**	**right iliac**	**left iliac**
sistole	-16,92316164	-19,63558495	-11,77606038	-29,12730605	-22,53789464
deceleration	-15,06569056	-15,95024318	-10,45289844	-32,83607739	-25,69508359
diastole	-2,147251816	8,878592766	-0,88369432	-58,67103519	-47,17660934

% Flow rate - Zero pressure outlet condition					
% NT post	**right renal**	**left renal**	**mesenteric**	**right iliac**	**left iliac**
sistole	-5,594700768	-10,16818402	-11,59651445	-34,3205305	-38,32007
deceleration	-3,600137911	-8,438621036	-9,987727838	-36,64410449	-41,32939199
diastole	5,217854364	10,33775911	13,63522993	-41,46448863	-87,72643396

% Flow rate - Profile pressure outlet condition					
% PE pre	**right renal**	**left renal**	**mesenteric**	**right iliac**	**left iliac**
sistole	-11,39282826	-7,305185924	-10,81031504	-34,4720595	-36,02603047
deceleration	-8,652054718	-5,668139698	-8,418070186	-35,21976833	-42,04027339
diastole	-3,757287596	-1,324124487	2,181608397	-50,34959202	-46,69431678

% Flow rate - Profile pressure outlet condition					
% PE post	**right renal**	**left renal**	**mesenteric**	**right iliac**	**left iliac**
sistole	-7,324622935	-10,92832444	-16,36610525	-34,12619379	-31,25499469
deceleration	-5,780147616	-8,904238654	-13,23818688	-37,96009456	-34,11610604
diastole	-4,88E-01	1,561474523	4,347177181	-57,02248906	-48,33790033

% Flow rate - Profile pressure outlet condition					
% NT pre	**right renal**	**left renal**	**mesenteric**	**right iliac**	**left iliac**
sistole	-17,51100156	-19,83341444	-11,65224065	-28,75605954	-22,24676091
deceleration	-15,78924301	-16,26497825	-10,32501446	-32,33441826	-25,28762796
diastole	-8,054680572	7,306410199	0,779994403	-55,36488831	-44,55636655

% Flow rate - Profile pressure outlet condition					
% NT post	**right renal**	**left renal**	**mesenteric**	**right iliac**	**left iliac**
sistole	-5,08341688	-10,44863201	-12,25792221	-34,06572441	-38,1431644
deceleration	-3,39878948	-7,867977937	-9,128177147	-36,88235427	-42,71895434
diastole	2,019947441	4,836707469	8,395942733	-43,88490243	-71,27983847

Table 1. % Flow rate in different outlet boundary conditions for patient PE and patient NT.

The arteries, both before and after the operation, are open and blood can flow inside them. Similar situations are observed for the two patients. The percentage flow rate is calculated for both outlet conditions, and between these, there are concordant results. Passing from systole to diastole, the renal and mesenteric arteries are supplied with a decreasing percentage of fluid; in the diastole phase in particular due to the non-pumping action of the heart. Passing from the pre-operative phase to the post-operative phase, a decrease in the percentage flow rate of the renal and mesenteric arteries is visible.

4 Discussion

EVAR is considered a technique of election for the treatment of patients suffering from abdominal aortic aneurysm thanks its low mortality and morbidity rate compare to open repair surgery.

Although with good results EVAR does not ensure the complete restoration of morphology and physiological hemodynamics (Zarins et al. 2009) in fact the hemodynamic devices on the market today are related to adverse events in post-operative situation, hence the need to study the impact of the device on the local hemodynamics in order to highlighting positive and negative expectations of a given stentgraft.

In order to carry out the analysis an economic method and able to provide accurate results is the computational fluid dynamics that generate computer experiments that, reducing the degrees of freedom of the system to a single parameter, simulate the trend of the blood flow (Raptis et al. 2019). In this study patient-based models have been realized and the focus has been on the study of pre and post operative hemodynamics of patients treated with CEVAR technique because they suffer from abdominal aortic aneurysm. CEVAR endovascular technique allows the introduction of a stent graft inside the abdominal aorta in the tract affected by the pathology following a minimally invasive procedure. The surgical operation is performed in order to exclude the aneurysm from the systemic circulation. The analysis was performed on two patients, for each one two different types of boundary conditions were explored.

In a previous work, models of two AAA patients were built and treated with FEVAR, the purpose of the surgical techniques is the same in order to restore the physiological hemodynamics.

A very important parameter, that is analyzed, is the Wall Shear Stress; a physiological profile of WSS helps to reduce the wall from atherogenesis and thrombus formation. On the other hand, in a preoperative situation, the oscillation of WSS due to geometry

can lead positively After the operation the values associated with WSS may indicate different situations: low WSS values lead, in the presence of stent graft, to the possibility of occlusion of the iliac arteries due to restenosis phenomena, this situation would lead to the need for the patient to undergo a reintervention (Papaioannou and Stefanadis 2005).

LNH reveals the presence of a core flow that envelops itself in a helical way and turns to the distal zone removing the disturbed flow zones and preventing the accumulation of substances (Gallo et al. 2012). The recirculation zones are dangerous from a clinical point of view as they favorite the aggregation of blood particles and the formation of thrombi that can obstruct the iliac and lead the patient to a new operation (Raptis et al. 2017). The helical flow facilitates blood transport and prevents the accumulation of low-density atherogenic lipoproteins on the vessel wall.

The data obtained from the OSI analysis show a significant improvement in the post-operative case, OSI indicates how much the flow changes direction during the cardiac cycle. In the pre-operative case, OSI values > 0.2 show a flow reversing its direction and are mainly observed in the aneurysmal zone and in the zone at the model inlet; these zones with high OSI may be subject to endothelial dysfunction. After the operation, in the pre aneurysmal zone, the OSI values decrease positively, however, the values near the renal and mesenteric arteries remain high; for this reasons these zones should be monitored. An important result is associated with the relationship between OSI and Relative Residence Time (RRT); in fact, a visual analysis shows that OSI and RRT have the same trend. RRT depends, according to its mathematical definition, on OSI and TAWSS but it can be observed that its behaviour depends more on the OSI trend. This result leads to think that an oscillatory flow can be related to the longer time the particles stay near the endothelium, in fact, being the oscillatory flow, the particles are not pushed in the distal direction.

Also the pressure is analysed in this work, the pressure drop drives the blood flow; a low pressure drop from the proximal to the distal position can be an indicator of stagnant flow and deceleration leading to all the consequences of the blood stasis. The

condition of low pressure drop is particularly noted in a preoperative situation; as a result of the operation a linear pressure drop from the renal to the iliac area is noted.

During this work, models of patients subject to AAA and treated with CEVAR have been realized also with the aim of comparing the CEVAR technique with FEVAR. In fact, a study on FEVAR was previously carried out with the same boundary conditions imposed in this case. The two techniques differ for the implantation methodology, CEVAR requires short device preparation time, for this reasons usually it is adopted during emergency process, while the FEVAR manufacturing process takes several months (Donas et al. 2013).

CEVAR can be used in case of urgent operation as the stents off the shelf allow the adaptation to the patient's anatomy. Patients treated with CEVAR are also exposed to contrast agent for less time and less blood loss than those treated with FEVAR (Li Y. et al. 2016).

Previous studies have shown that 30-day mortality is lower in the case of FEVAR (2.4% in the case of FEVAR and 5.3% in the case of CEVAR); 6 months mortality was higher in FEVAR (13%) than in CEVAR (7%) (Katsargyris et al, 2013). Other medical issues found during the follow-up of previous studies are renal failure, and pulmonary or cardiac complications, with higher percentage in CEVAR (Katsargyris et al, 2013). In addition, the literature shows that there is a reduction in renal artery perfusion in patients undergoing FEVAR; this result is due to the relatively long curved length of the chimney grafts through which the flow takes place, to the reduced cross section area of the secondary grafts because of the compression with the main lumen stent-graft and to the losses that occur due to changes in flow direction.

Even if FEVAR seems to have less implications compared to CEVAR, concerning the computational part of this study and the comparison with the previous one, the following aspects can be highlighted. The obtained results in both designs, CEVAR and FEVAR, show overall improvement in hemodynamic parameters from the pre-operative to the post-operative cases. There is a significant decrease in pressure in the

area of the aneurysm post-operatively in both designs. This behavior is due to the substantial geometric modification after the CEVAR of FEVAR stent implantation. The results obtained for LNH in this study are in line with those obtained in the FEVAR study that considered an $|LNH| < 0.2$.

Related to the OSI, the WSS increases as a result of the surgical intervention, guaranteeing the absence of recirculation zones that would be a favorable condition for thrombus formation. The findings of the FEVAR study showed that the flow in the superior mesenteric and renal arteries remains almost unaffected after intervention retaining all important indices to normal levels. Low WSS values in the main part of the stent and high values in the physiological area of the aorta and near the renal and mesenteric areas can also be observed in simulations performed for FEVAR (Malatos et al, 2019).

The same OSI trend can be found in the previous FEVAR study, although in this case, even in the post-operative situation, OSI values remain higher in the area where the aneurysm was in comparison with the post-CEVAR situation (Malatos et al. 2019). This behavior could suggest that these specific FEVAR regions are more sensitive to flow separation and probably may become prone to thrombus formation.

In the realization of this work, hypotheses have been made that influence the results achieved; in particular the vascular wall is assumed to be rigid, in reality there are changes in shape during the cardiac cycle, it would be appropriate to realize a variable geometric model during the simulations.

Although a non-rigid model can be realized, the hypothesis of vascular wall rigidity does not influence the results in an unacceptable way in fact endovascular surgery for AAA repair are performed on old patients who, compared to young patients, have a rigid wall. In addition, the aneurysm being analyzed is in the abdominal position, the abdominal aorta has a low concentration of elastin compared to that present in other areas, such as the thorax area.

Moreover, from the point of view of simulation, meshes with a greater number of elements can be built and the differences between different meshes can be studied. Other parameters can be explored to investigate the risk of device migration due to displacement forces acting on the stent graft wall and to calculate the recirculation volume to analyze areas with disturbed hemodynamics.

In future studies may be conducted to statistically correlate the geometric characteristics of the patient and hemodynamic parameters; other studies may be conducted to explore the CEVAR technique in more depth, the cohort of patients included in this study may be expanded in order to obtain statistically acceptable results, also in order to improve the design of the devices to be implanted. In addition, the models have been developed on pre-operative and post-operative situations at one month, follow-up at six or twelve months may confirm the results obtained.

5 Conclusions

Nowadays it is more and more necessary to realize patient-based treatments for aortic aneurysms in abdominal aorta, so patient based modelling is a very promising tool for the study and understanding of hemodynamic parameters that then influence the decisions taken by clinicians in pre- and post-operative phases. (Kostantinos et al, 2019).

This study shows the correlation between hemodynamic parameters and adverse events that may occur in the patient. A close correlation between OSI and RRT is shown. Analyzing the studied parameters, hypotheses can be made about the risk of thrombus formation and device migration in the post-operative phase.

In a previous study, simulations were carried out parallel to those carried out for the present study for a different endovascular surgical technique. The results are encouraging in both techniques as there is an improvement in all parameters. Patient-based modelling could provide support to the clinician and indicate which technique to use based on mathematical results obtained in each case.

In conclusion we suggest, in order to obtain more accurate and statistically valid results we suggest the in-depth study of the follow up after one month of the patients analyzed in this work, in particular it is recommended to monitor the geometric characteristics, its variations during time and the resulting helical flow.

6 References

Alastruey J., K. H. Parker, Joaquim Peiro, Spencer J. Sherwin, *Lumped parameter outflow models for 1-D blood flow simulations: Effect on pulse waves and parameter estimation*, Communications in Computational Physics 4(2):317-336, August 2008.

Anastasios Raptis, Michalis Xenos, Efstratios Georgakarakos, George Kouvelos, Athanasios Giannoukas, Nicos Labropoulos, Miltiadis Matsagkas, *Comparison of physiological and post-endovascular aneurysm repair infrarenal blood flow* in *Computer Methods in Biomechanics and Biomedical Engineering*, 2007 pag 20:3, 242-249, DOI:10.1080/10255842.2016.1215437.

Anastasios Raptis, Michalis Xenos, Konstantinos Spanos, George Kouvelos, Athanasios Giannoukas, Miltiadis Matsagkas*, Endograft Specific Haemodynamics After Endovascular Aneurysm Repair: Flow Characteristics of Four Stent Graft Systems* in *2019 European Society for Vascular Surgery*.

Bailey R., Anatomy of the heart: valves, DOI: https://www.thoughtco.com/anatomy-of-the-heart-valves-373203.

Brant W. Ullery, MD,a Ga-Young Suh, PhD,a Jason T. Lee, MD,a Brian Liu, *Geometry and respiratory-induced deformation of abdominal branch vessels and stents after complex endovascular aneurysm repair*, J Vasc Surg. 2015 Apr;61(4):875-84. doi: 10.1016/j.jvs.2014.11.075.

Callanan, Anthony & Davis, NIALL & Walsh, Michael & Mcgloughlin, Tim. (2011). *Tissue-Engineered Extracellular Matrices (ECMs) as Adjuvant Scaffolds for Endovascular Aneurysmal Repair (EVAR).* 10.5772/21334.

Campo-Deaño L, Oliveira MN, Pinho FT. *A Review of Computational Hemodynamics in Middle Cerebral Aneurysms and Rheological Models for Blood Flow*. *Appl. Mech. Rev.* 2015, Vol. 67, 3, pp. 030801-16.

Clinical Practice Guidelines for Endovascular Abdominal Aortic Aneurysm Repair: Written by the Standards of Practice Committee for the Society of Interventional Radiology and Endorsed by the Cardiovascular and Interventional

Cooper A, *Endovascular Repair of Abdominal Aortic Aneurysm.*

Dangas George, David O'Connor, Belal Firwana, Somjot Brar, Sharif Ellozy, Angeliki Vouyouka, Margaret Arnold, Constantine E. Kosmas, Prakash Krishnan, Jose Wiley, Javed Suleman, Jeffrey Olin, Michael Marin and Peter Faries: *Open Versus Endovascular Stent Graft Repair of Abdominal Aortic Aneurysms* in JACC: Cardiovascular Interventions, October 2012, vol. 5 no. 10 1071-1080, Doi: 10.1016/j.jcin.2012.06.015.

David A. Steinman, *Image-Based Computational Fluid Dynamics Modeling in Realistic Arterial Geometries*, in *Annals of Biomedical Engineering,* Vol. 30, pp. 483–497, 2002.

Donas KP, Pecoraro F, Bisdas T, Lachat M, Torsello G, Rancic Z, Austermann M, Mayer D, Pfammatter T, Puchner S. "*CT angiography at 24 months demonstrates durability of EVAR with the use of chimney grafts for pararenal aortic pathologies"*, J Endovasc Ther. 2013 Feb;20(1):1-6. doi: 10.1583/12-4029.1.

Eduardo Soudah, E. Y. K. Ng, T. H. Loong, Maurizio Bordone, Uei Pua, and Sriram Narayanan. *CFD Modelling of Abdominal Aortic Aneurysm on Hemodynamic Loads Using a Realistic Geometry with CT* in *Computational and Mathematical Methods in Medicine.* 2013, Vol. 2013, 472564.

Eric Ducasse, MD; Caroline Caradu, MD; Xavier Berard, MD; Gerard Sassoust, MD; Dominique Midy, MD, *Meta-Analysis of Chimney vs Fenestrated Endovascular Aneurysm Repair for Complex Aortic Aneurysm*, Department of Vascular Surgery, University of Bordeaux, University Hospital of Bordeaux, Bordeaux, France, Volume 13 - Issue 12 - December 2016.

Gallo, D., Steinman, D. A., Bijari, P. B. and Morbiducci, U., 2012. *Helical flow in carotid bifurcation as surrogate marker of exposure to disturbed shear. Journal of Biomechanics*. 45(14), 2398-2404.

Gedmintas, M. grabove, P. Atkinson, "*My patient has no blood pressure: Have they got an abdominal aortic aneurysm? Point-of-care ultrasound of the abdominal aorta in hypotensive patients*", November 2011, Ultrasound 19(4):236-241, DOI: 10.1258/ult.2011.010048.

Hiroshi B., Frédéric Cochennec, Jean Marzelle, Jean-Pierre Becquemin, *Comparison of fenestrated endovascular repair and chimney graft techniques for pararenal aortic aneurysm*, Journal of Vascular Surgery, Volume 60, Issue 1, 31 – 39, 2014.

Hyun Jin Kim, Figueroa, C. Alberto, Vignon-Clementel, Irene E., Jansen, Kenneth E., and Taylor, Charles A. "*On Coupling a Lumped-Parameter Heart Model With a Three-Dimensional Finite Element Model of the Aorta*." *Proceedings of the ASME 2007 Summer Bioengineering Conference. ASME 2007 Summer Bioengineering Conference.* Keystone, Colorado, USA. June 20–24, 2007. pp. 317-318. ASME. https://doi.org/10.1115/SBC2007-175536.

Juan C. Lasheras, *The Biomechanics of Arterial Aneurysms* in *The Annual Review of Fluid Mechanics* 2007, 39:293–319. Available online 10.1146/annurev.fluid.39.050905.110128, pag 1-18.

K. Shawky, "*Controversies in hostile neck management of AAA: solutions from real life experience*", 2019,DOI:https://static.livemedia.gr/services/conferre/userfiles/usid0_20190511132905_live2019yournameyourpresentationtitlecopy132905.pdf.

K.P. Donas, Markus Eisenack, G. Panuccio, M. Austermann, N. Osada, G. Torsello, *The role of open and endovascular treatment with fenestrated and chimney endografts for patients with juxtarenal aortic aneurysms,* Journal of Vascular Surgery Volume 56,Issue 2; August 2012, Pages 285-290 **.**

Katsargyris, A., Oikonomou, K., Klonaris, C., Töpel, I., & Verhoeven, E. L. G. (2013), *Comparison of Outcomes With Open, Fenestrated, and Chimney Graft Repair of Juxtarenal Aneurysms: Are We Ready for a Paradigm Shift?,* Journal of Endovascular Therapy, 20(2), 159-169. https://doi.org/10.1583/1545-1550-20.2.159.

Kira N. Long, MD; Ross Milner, MD, *The chimney thecnique for juxtarenal aortic aneurism*, University of Chicago Medicine & Biological Sciences, Chicago, Illinois. Volume 13 - Issue 9 - September 2016.

Konstantinos G. Moulakakis, John Kakisis,, Eleni Gonidaki, Dipl Eng, *Comparison of Fluid Dynamics Variations Between Chimney and Fenestrated Endografts for Pararenal Aneurysms Repair: A Patient Specific Computational Study as Motivation for Clinical Decision-Making,* Vascular and Endovascular Surgery 2019, Vol. 53(7) 572-582 DOI:10.1177/1538574419867531 journals.sagepub.com.

Lantz, Jonas, *On Aortic Blood Flow Simulations*. Linkoping, Sweden: Department of Management and Engineering, 2013.

Lanzoni S., *Le equazioni della meccanica dei fluidi,* Dipartimento di Ingegneria Idraulica, Marittima e Geotecnica Università di Padova.

Li, Y., Hu, Z., Bai, C. *et al. Fenestrated and Chimney Technique for Juxtarenal Aortic Aneurysm: A Systematic Review and Pooled Data Analysis*. *SciRep* 6, 20497(2016). https://doi.org/10.1038/srep20497.

Lombardo, Agostino, *Indagine diagnostica sulle complicanze in seguito a un intervento di Endoprotesi per aneurisma dell'aorta addominale: L'Endoleak.*2009/2010.

Luca Antiga, Marina Piccinelli, Lorenzo Botti, Bogdan Ene-Iordache, Andrea Remuzzi, David A. Steinman, *An image-based modeling framework for patient-specific computational hemodynamics* in *Med Biol Eng Comput 46*, 2008 pag:1097–1112 DOI 10.1007/s11517-008-0420-1.

Malatos S, Raptis A, Xenos M (2016) *Advances in Low-Dimensional Mathematical Modeling of the Human Cardiovascular System,* J Hypertens Manag 2:017. 10.23937/2474-3690/1510017.

Maldonado T., Fenestrated versus Chimney Endovascular Aortic Aneurysm Repair, Rev Argent Cardiol 2018;86:185-189. http://dx.doi.org/10.7775/rac.v86.i3.11905.

Malek AM, Alper SL, Izumo S. *Hemodynamic shear stress and its role in atherosclerosis* in *JAMA 1999*;282:2035-42.

Mital Desai, James Eaton-Evans, Claire Hillery, Raheleh Bakhshi, Zhong You, Jian Lu, George Hamilton, Alexander Seifalian, *AAA Stent–Grafts: Past Problems and Future Prospects* in *Annals of Biomedical Engineering*, Vol. 38, No. 4, April 2010 (2010) pp. 1259–1275 DOI: 10.1007/s10439-010-9953-1..

Morbiducci U, Ponzini R, Gallo D, Bignardi C, Rizzo G*., Inflow boundary conditions for image-based computational hemodynamics: impact of idealized versus measured velocity profiles in the human aorta,* J Biomech. 2013 Jan 4;46(1):102-9. doi: 10.1016/j.jbiomech.2012.10.012.

Morbiducci U., *Biomeccanica del sistema cardiovalscolare*, 2019, Torino.

N. van de Vosse F., Nikos Stergiopulos, *Pulse Wave Propagation in the Arterial Tree*, Annual Review of Fluid Mechanics, Vol.43:467-499, 2011.

Nan Xiao a,c, Jay D. Humphrey b, C. Alberto Figuero, *Multi-scale computational model of three-dimensional hemodynamics within a deformable full-body arterial network*, https://doi.org/10.1016/j.jcp.2012.09.016.

Ohrlander, T, Sonesson, B., K. Ivancev, T. Resch, N. Dias, M. Malina, *The chimney graft: a technique for preserving or rescuing aortic branch vessels in stent-graft sealing zones*, J Endovasc Ther. 15(4): 427-32, 2008.

Olufsen, M.S., Peskin, C.S., Kim, W.Y. *et al. Numerical Simulation and Experimental Validation of Blood Flow in Arteries with Structured-Tree Outflow Conditions*. Annals of Biomedical Engineering 28, 1281–1299 (2000). https://doi.org/10.1114/1.1326031.

Pankaj K. Singh Alberto Marzo Bethany Howard Daniel A. RufenachtPhilippe Bijlenga Alejandro F. Frangi Patricia V. Lawford Stuart C. ColeyD. Rodney Hose Umang J.*Patel, Effects of smoking and hypertension on wall shear stress and oscillatory shearindex at the site of intracranial aneurysm formation* in Clin Neurol Neurosurg. 2010, 112(4):306-13. DOI: 10.1016/j.clineuro.2009.12.018.

Papaioannou TG, Stefanadis C. 2005. *Vascular wass shear stress: basic principles and methods*. Hellenic J Cardiol. 46:9-15.

Paulson W., Jones S., A., *Hemodynamics of the Hemodialysis Access: Implication for Clinical Management,* February 2004 Contributions to Nephrology 142:238-53.

Pedley, T. J. (1997). *Introduction to Fluid Dynamics*, 61(1), 7â24.

Philippe Reymond, Fabrice Merenda, Fabienne Perren, Daniel Rüfenacht, Nikos Stergiopulos *Validation of a one-dimensional model of the systemic arterial tree*, 01 JUL 2009https://doi.org/10.1152/ajpheart.00037.2009.

Pornhatai K.t Pasuk M., and Srijit D. *Morphology of the human aorta and age-related changes: anatomical facts* in *Anat Cell Biol,* 2019 Jun; 52(2): 109–114. Published online 2019 Jun 30. doi: 10.5115/acb.2019.52.2.109 Published online 2019 Jun 30. doi: 10.5115/acb.2019.52.2.109.

Prinssen E. Buskens J. D. Blankensteijn *Quality of Life after Endovascular and Open AAA Repair.Results of a Randomised Trial* in Eur J Vasc Endovasc Surg27, 121–127 (2004) DOI: 10.1016/j.ejvs.2003.11.006.

S.J. Sherwin, V. Franke, J. Peiró, K. Parker, *One-dimensional modelling of a vascular network in space-time variables*, J. Eng. Math. 47:217–50 2003.

Sean A. Crawford, MD, MSc,a,bRyan M. Sanford, BScE,cThomas L. Forbes, MD,b,dCristina H. Amon, ScD,a,candMatthew G. Doyle, PhD,cToronto, Ontario, Canada, *Clinical outcomes and material properties of in situfenestration of endovascular stent grafts*, J Vasc Surg. 2016 Jul;64(1):244-50. doi: 10.1016/j.jvs.2016.03.445).

Stavros Malatos, Anastasios Raptis, Michalis Xenos, George Kouvelos, Athanasios Katsargyris, , Athanasios Giannoukas, Erik L. Verhoeven, Miltiadis Matsagkas, *A multiscale model for hemodynamic properties' prediction after fenestrated endovascular aneurysm repair. A pilot study* in Hellenic Journal of Vascular and Endovascular Surgery, 2019, vol1 Issue 2 pag 73-78.

Stergiopulos N., D.F.Young, T.R.Rogge, *Computer simulation of arterial flowwith applications to arterial and aortic stenoses*, J. Biomech. 25:1477–88, https://doi.org/10.1016/0021-9290(92)90060.

Tittel K. *Anatomia funzionale dell' uomo*, edi.emes,edizione italiana G. Marinozzi, pag 400-450.

Vignon-Clementel I., C.Alberto Figueroa, Kenneth E.Jansen, Charles A.Taylor, *Outflow boundary conditions for three-dimensional finite element modeling of blood flow and pressure in arteries*, Volume 195, Issues 29–32, 1 June 2006, Pages 3776-3796, https://doi.org/10.1016/j.cma.2005.04.014.

Wicky S, Kundu S, Drescher P, d'Othee BJ, Rose SC, and Cardella JF. J Vasc Interv Radiol 2010; 21:1632–1655. ©SIR,2010.

Zarins, C. K. and Taylor, C. A., 2009. Endovascular Device Design in the Future: Transformation From Triam and Error to Computational Design. Journal of Endovascular Therapy.